SLAC – PUB – 3407
August 1984
(T/E)

Z^0 DECAY MODES – EXPERIMENTAL MEASUREMENTS*

J. M. DORFAN
Stanford Linear Accelerator Center
Stanford, California 94305

TABLE OF CONTENTS

---

* Work supported by the Department of Energy, contract DE-AC03-76SF00515.

Lecture Presented at the Theoretical Advanced Study Institute on Elementary Particle Physics, Ann Arbor, Michigan, June 4 – 29, 1984.

1. INTRODUCTION

This report summarizes three lectures given at the Theoretical Advanced Study Institute at the University of Michigan at Ann Arbor. The audience was exclusively theory graduate students many of whom had little if any knowledge about accelerators, detectors and analysis techniques. In presenting a lecture series "Z^0 Decay Modes – Experimental" I felt it was my task to introduce the students to the future Z^0 machines and detectors and cover, in not too much detail, how these tools could be used to investigate the physics of Z^0 decays. This writeup reflects the attitude which I took in my lectures, and I have in no way tried to broaden my goals, make explanations more complete or service a broader, more experimentally based readership. In many cases the students received detailed theoretical lectures on topics covered by these lectures and I was able to benefit from these lectures by omitting background material. In that context I have not made an effort to make this writeup complete – I hope it is useful as a chapter in the proceedings of the TASI Summer School.

The lectures begin with an introduction to storage rings and linear colliders with special reference to the parameters of the SLC and LEP. The rigors of the Z^0 environment are presented in section 3 along with the requirements for SLC and LEP detectors. In section 4, I develop the pedagogy needed for testing the Standard Model and in section 5 some experimental tests of the Standard Model are discussed. In section 6, I discuss tests which involve extensions of the Standard Model (charged Higgs particles, more generations) as well as a few examples of how supersymmetry may show up at the Z^0.

I have used many sources in preparing these lectures – most of these are cited as references. In particular I borrowed extensively from Gary Feldman's CERN COURS/LECTURE series entitled "Spectroscopy of of New Particles with e^+e^- Colliders" and Chris Quigg's book "Gauge Theories of the Strong, Weak and Electromagnetic Interactions." Both of these texts offer splendid background material for these lectures.

2. THE Z^0 MACHINES

To study most of the physics covered by these lectures we will require large numbers ($\gtrsim 10^5$) of Z^0 decays. We will also want to have an environment in which there is a minimal loss of decay channels arising from trigger and/or analysis techniques. The $\bar{p}p$ machines will provide valuable information about the Z^0, but the number of events will be sparse and all the Z^0 decay channels are not analyzable. As of now the UA1 and UA2 detector groups have less than 20 identified Z^0 events all of which are in the decay channel $Z^0 \to e^+e^-$ or $\mu^+\mu^-$.

The high energy physics community is constructing two machines capable of providing $\simeq 10^6$ Z^0's per year. The LEP machine is under construction at CERN and the SLC machine is being built at SLAC. These two Z^0 "factories" are quite different machines and they offer different experimental possibilities. The LEP machine is a conventional e^+e^- storage ring – a scaled up version of PETRA at DESY and PEP at SLAC. It uses well understood, proven technology and should perform close to its design specifications shortly after beam turn–on. The SLC (Stanford Linear Collider) uses an entirely new concept in accelerator technology and, in that sense, is a less certain path to high luminosity. However as we will see, the SLC is a pioneering effort in the area of linear colliders which provide the only affordable means to TeV e^+e^- colliding beam physics. The SLC will serve both as a prototype for future very high energy colliding linacs and as a copious source of Z^0's. How do the two approaches differ?

2.1 Conventional e^+e^- Storage Rings

In a conventional e^+e^- storage ring one or more bunches of electrons and positrons are stored, travelling in opposite directions in a magnetic guide field. Collisions occur at fixed points around the ring (so called interaction regions) and there are $2n_b$ collision points possible where n_b is number of bunches. The particle detectors are placed in the interaction regions. The magnetic guide field comprises a) dipoles which provide the restoring force for a closed $e^\pm$ orbit b) quadrupoles for focussing the e^+e^- beams and c) sextuples to remove or reduce chromatic abberations in the magnetic focussing system.

Storage rings suffer substantial energy loss from synchrotron radiation. An electron of energy $E_{\rm beam}$ travelling in a circle of radius R loses an amount

$$\Delta E = 88.5 \times 10^{-6} \ \ (\text{metre GeV}^{-3}) \ \ \frac{E^4_{\rm beam}}{R} \qquad (1)$$

of energy per revolution. An $e^\pm$ at PEP loses about 10 MeV/revolution for $E_{\rm beam}$ = 14.5 GeV. This power must be restored by RF cavities placed at strategic points around the storage ring. At full current (40 mamps) the PEP machine requires 6 MW of RF power. It is important to notice the $E^4_{\rm beam}$ dependence in the synchrotron radiation loss – there is a <u>substantial</u> penalty paid as one raises the beam energy of a storage ring.

The rate for a process with cross section σ is

$$\text{rate} = \mathcal{L}\,\sigma$$

where $\mathcal{L}$ is the luminosity measured typically in units of $cm^{-2}\ sec^{-1}$. For the

collision of an e^+ and e^- bunch, the luminosity is given by

$$\mathcal{L} = \frac{N^+ N^- f}{A} \tag{2}$$

where $N^\pm$ is the number of $e^\pm$/bunch, f is the collision frequency and A is the area of the larger of the two beams. Typical luminosities for existing storage rings are $\simeq 10^{31}\ cm^{-2}\ sec^{-1}$. The luminosity does not grow without bound; as one adds increasing amounts of $e^\pm$ to the beams, the continuous passage of one beam through the other causes one or both of the beams to grow, thereby reducing the luminosity. It is the cumulative effect of many small perturbations that causes the beam–beam interaction to limit the luminosity. In addition one can only tolerate as much beam current as one has RF power to suitably restore the energy lost to synchrotron radiation.

Typical beam sizes in a storage ring are

$$\sigma_x \approx 500\ \mu m$$

$$\sigma_y \simeq 50\ \mu m$$

and $$\sigma_z \simeq 2\ cm$$

where x is the coordinate in the direction of the dipole magnet field (i.e. horizontal), y is vertical and z is measured along the beam direction. The beam size is limited by the synchrotron radiation damping and excitation, again a process resulting from the multiple revolution nature of the machine.

What limits the center of mass energy ($E_{\text{c.m.}} = 2E_{\text{beam}}$) achievable with storage rings? It turns out that the economics of very high energy storage rings is very unfavorable. We can write the equation for the cost (C) of a storage ring as

$$C = \alpha R + \beta \frac{E_{\text{beam}}^4}{R} \tag{3}$$

where α and β are constants and R is the radius of the machine. The first term in the cost equation arises from elements needed to build the ring – tunnels, vacuum system, ring magnets etc. The second term comes from the RF system (see equation 1). Let us suppose that we minimize the cost as a function of radius R. Differentiating and setting $dC/dR = 0$ one finds

$$R = (\beta/\alpha)^{1/2}\ E_{\text{beam}}^2$$

$$C = 2(\beta/\alpha)^{1/2}\ E_{\text{beam}}^2\ .$$

Hence the cost of the construction of a storage ring scales like E_{beam}^2 as does the radius (real estate). Lets look at some concrete examples starting with the

LEP machine as a guide. The first phase of LEP will be a 50×50 GeV machine with conventional RF, circumference = 27 km and $C = \$500\ M$. Suppose we scaled this up to a 500×500 GeV machine: circumference $\rightarrow$ 2700 km and $C \rightarrow \$50,000\ M$! Clearly such a machine is prohibitively expensive. Can one improve the situation by using superconducting RF? The second (superconducting) phase of LEP will be a 100×100 GeV machine at a cost of about $\$700\ M$. Hence using superconducting RF our 500×500 GeV machine will have parameters circumference = 675 km and $C = \$17,500\ M$ – still far too costly! So clearly we need a different technology to pursue e^+e^- physics in the TeV energy range. This brings us to option 2.2.

2.2 THE LINEAR e^+e^- COLLIDER

In a linear collider machine one envisages two linear accelerators firing beams of electrons and positrons at each other. Following the collision, the beams are discarded. The detector is placed at the collision point. In such a machine the cost will scale like E_{beam} : $C = \alpha' E_{\text{beam}}$ and one gets away from the E^2_{beam} scaling law of the storage ring. If one started building machines from scratch (no existing accelerator facilities) the constants α, β and α' are such that the cost of the linear collider and a storage ring are equal at roughly $E_{\text{c.m.}} \approx 150 - 200$ GeV. Above this energy range the linear collider becomes increasingly more economical. How does one achieve useful luminosities in a linear collider? The luminosity is given by equation 2. For LEP $f \approx 50,000$ while for a linac (SLAC) $f \approx 200$. In a storage ring one uses a linac to repeatedly add current to the $e^{\pm}$ bunches until a bunch in the storage ring contains many orders of magnitude more $e^{\pm}$ than a single linac bunch. Hence N^+N^- is several orders of magnitude larger in the storage ring than for linear colliders. The only way then to get a luminosity comparable to a storage ring is to reduce the beam size A in the collider by about 10^5 relative to the beam size in the storage ring. As discussed earlier the beam size in a storage ring is limited by the synchrotron radiation losses. The colliding linac does not suffer from this problem – the beam size is limited by the emittance of the linac beam. The emittance can be controlled to yield beam sizes on the order of 10 $(\mu m)^2$. Hence, in principle, the reduction in frequency and bunch particle number density can be largely offset by the reduction in beam size and a colliding linac luminosity of $\approx 10^{31}$ should be possible.

The dynamics of the beam–beam interaction is very different in colliding linacs than in a storage ring. This problem is discussed fully in reference 1. The major difference comes about from the fact that the charge density in the colliding linacs is considerably (several orders of magnitude) higher than in a storage ring. The maximum current which can be collided in the colliding linac machine will still be limited by the beam–beam interaction. However the nature

of the beam–beam interaction is very different in the colliding linac. The collision of the two high current density beams is very disruptive and tends to blow the beams apart. For sufficiently high currents (charge density) the passage of the one beam through the other causes a reduction (focusing) of beam size prior to the destructive disruption of the beams. This so–called "pinch" effect therefore enhances the luminosity in a linear collider system. Figure 1 (taken from reference 1) shows the pinch effect graphically. Four "snapshots" of the beam profiles in x, transverse to the beam, and z, along the beams, are shown. The upper two snapshots are taken as the e^+ and e^- beams approach each other. The third snapshot shows dramatically how the beam size has been squeezed down and in the forth the beams have passed "through" each other and are beginning to "explode." In a machine like the SLC, the "pinch" effect is expected to produce a factor of ~ 6 increase in luminosity. As stated before, linear colliders are an untested technology – the problems of producing and colliding micron size beams are by no means solved. However they will receive their first real test with the commissioning of the SLC.

The LEP Machine

LEP will be a conventional e^+e^- storage ring and a comprehensive description can be found in reference 2. The ring is being built at CERN and will have a circumference of 27 km. In its first incarnation (LEPI) it will achieve a maximum collision energy of 100 GeV and a luminosity of $10^{31}\ cm^{-2}\ sec^{-1}$. 16 MW of conventional RF will be required for LEPI and the machine is expected to deliver collisions in late 1988. The initial outlay for LEP will be \$500 M and it will have eight experimental halls – four of which will be instrumented at the beginning. The initial detectors go by the names of LEP3, OPAL, DELPHI and ALEPH. Typically these detectors will cost \$50 M to build.

The LEPI machine will be upgraded to $E_{\text{c.m.}} \sim 170$ GeV by the addition of 80 MW of RF power and then to $E_{\text{c.m.}} \approx 250$ GeV using superconducting RF cavities. The time scale for these upgrades is not yet known. Since the LEPI machine relies on conventional techniques, design performance should be reached soon after the first collisions.

The SLC Machine

The SLC machine is being built at SLAC and is slated to deliver colliding beams at the Z^0 in late 1986. The design luminosity of the machine is $6 \times 10^{30}\ cm^{-2}\ sec^{-1}$ and the maximum energy at turn–on will be 100 GeV. A complete description of the SLC can be found in reference 3. However, since the SLC is not a conventional e^+e^- storage ring, we provide here a short description of the machine referring to figure 2. The existing linac will be upgraded to 50 GeV using an extension of the SLED ideas which enabled SLAC to raise the linac energy from 22 GeV to 34 GeV. An electron bunch is diverted out of the linac and collided with a target to produce positrons. These positrons are then fed

back into the front end of the accelerator. Following passage through damping rings, which provide cooling for the electron and positron bunches, a bunch of positrons immediately followed in the next linac bucket by a bunch of electrons, is transported down the accelerator to the colliding arcs. The positrons and electrons are switched to different arcs and are brought into collision by an elaborate system of optics, termed the final focus. Following the collision, the beams are dumped. So unlike a storage ring, the SLC operates as a single pass collider. The repetition rate of the linac is 180 Hz, many orders of magnitude less than that of typical storage rings. To produce a usable luminosity, this slow collision rate will be compensated for using an intense electron gun capable of producing 5×10^{10} electrons per bunch and by designing the final focus optics such that the transverse dimensions of the colliding beams are a few microns. The expected luminosity as a function of collision energy is shown in figure 3. The SLC is optimized to run at the Z^0 . However, the luminosity remains good down to energies of 60 GeV. If toponium is beyond the reach of the TRISTAN machine,[4] the SLC could be used to study toponium. The energy spread of the SLC machine will be about 0.4% at full luminosity and about 0.1% at a somewhat reduced luminosity. This can be compared with LEP which will have an energy spread of 0.1%.

Another feature of the SLC is the promise of longitudinally polarized beams, which, as we shall discuss, is a powerful tool for the study of Z^0 physics.[5] Polarized electrons are produced by shining circularly polarized laser light on a gallium arsinide cathode. Such an electron gun exists and has been successfully tested. Polarized electrons have already been transported down the linac and simulations of transport through the SLC arcs indicate that the transmission efficiency for the polarized electrons is $\geq 80\%$. The sign of the laser polarization can be reversed on a linac pulse by pulse basis yielding successive beam pulses of opposite polarizations. Hence it appears that, with very high probability, beams with polarizations of $\geq 50\%$ will be available at the SLC. Beam polarization at LEP is much less certain. The problems of producing and retaining the longitudinal polarization are many and no good solutions exist at this time. (See reference 2, page 132.)

The SLC machine has the distinct disadvantage of having only one interaction region. Because of the newness of the technology, it will take a considerable time and machine physics effort to reach design luminosity. The first detector for the SLC will be an upgraded MARK II detector. This detector will undergo a year of testing at PEP prior to installation at the SLC. A LEP competitive detector, the SLD, is also being designed. This detector is scheduled to begin physics running at the SLC in late 1988 and once it has been checked out it will replace the MARK II.

What about the event rate at the Z^0? As we will see in section 4, the cross section running on the Z^0 is about 50 nb. However initial state radiation reduces this to a usable cross section of about 40 nb. Assuming an average luminosity of $1.5 \times 10^{30}\ cm^{-2}\ sec^{-1}$, one finds an event rate of 5200 Z^0/day! Assuming 200 days for physics one has an event rate of 10^6 Z^0/year. During these lectures we will use this as a benchmark for calculating rates. Realistically during its first year, the SLC might achieve 10^5 Z^0 's, corresponding to an average luminosity of $1.5 \times 10^{29}\ cm^{-2}\ sec^{-1}$.

3. THE Z^0 ENVIRONMENT – REQUIREMENTS FOR DETECTORS

So it seems we will have two fine Z^0 "factories" – what kind of detectors do we need? The Z^0 environment has been studied in many workshops and the interested reader can find summaries of these workshops in reference 6 and reference 2. We describe here the main features of the environment, particularly as they pertain to detector design. The basic production process is shown in figure 4 where the final state particle naming convention is given in the figure caption. We now consider how these produced states decay. The final states e^+e^-, $\mu^+\mu^-$ are stable and result in opposite sign, high energy ($\gtrsim$ 40 GeV) back to back leptons. The typical decays of the other produced states are shown schematically in figure 5. A quick glance at figure 5 and one realizes that one needs at the Z^0 a detector capable of a) measuring the properties of high energy jets b) measuring and tagging electrons and muons over a wide range of momenta both in isolation and in the presence of high energy jets and c) measuring the total energy and momentum in the event as an indicator of the missing energy and transverse momentum of ν's.

In addition these are many multi-jet and multi-lepton events which demands that the detector be uniformly instrumented over as large a solid angle as possible. Figure 6 shows the fractional momentum carried by hadrons, leptons and photons in events of the type $Z^0 \rightarrow$ hadrons. Notice the large dynamic range of the particle momenta. The detector must do an equally good job at high and low momenta. The high momentum (leading) particles carry information about the quark flavor and the fragmentation process, while the intermediate and low energy particles provide information about the decay chains and the energy flow. Typical multiplicities for the $Z^0 \rightarrow$ hadrons are 22 charged particles and 23 photons per event – jet multiplicities on the order of 11 charged particles and 11 photons. In addition this multiplicity is highly collimated – most jets are contained in a $\lesssim 10^\circ$ cone. Figure 7 shows the angle between various particle species and the event jet axis. The distribution peaks at $\sim 2^\circ$ for photons and hadrons. Hence a detector will have to possess fine segmentation both in the charged tracking and the calorimetry.

Studies[6] of reconstruction of K_S^0, D^0, $D^{\pm}$, measurement of the invariant cross section $Sd\sigma/dx$ (at high x), measurement of the $\tau^{\pm}$ polarization lead to the conclusion that a momentum resolution of $\sigma_p/p \lesssim 0.3\ P$ (GeV/c) is needed. In order to separate leptons from hadrons cleanly will require rejection of hadrons at a level of $\geq 10^3$. This can be understood in simple terms as follows. The average charge multiplicity is 10/jet and the typical semi-leptonic branching fraction ($B(q \rightarrow \ell^{\pm}\ \nu\ x)$) is 10%. Hence in hadronic events one will have, on average, one $e^{\pm}$, $\mu^{\pm}$ per 100 charged hadrons. Having a signal to noise of 10 $e^{\pm}$, $\mu^{\pm}$ per 1 hadron requires a rejection of hadrons at the 10^3 level. A final requirement for a good detector in the new energy regime of the Z^0, is the ability to search for free quarks. This can be done by a) measuring the ionization of charged particles in a gas chamber (dE/dx) which measures charge directly or by b) using time of flight to look for massive particles.

It seems possible to design 4π detectors which are equal to most of the rigors of the environment described here. Although diverse in their approaches to the problems, the four LEP detectors and the SLD should do an excellent job of studying the Z^0 physics. The MARK II upgrade is a more modest approach designed to be ready for the early start of the SLC. Its main drawback is its lack of hadron calorimetry. However as a survey detector, it will do most physics very well. For completeness a list of the detector proposals is given in reference 7 and a schematic of the upgraded MARK II detector is given in figure 8.

4. THE STANDARD MODEL AND ITS APPLICATION TO $e^+e^- \rightarrow Z^0 \rightarrow f\bar{f}$

For most of these lectures we will assume the standard model. During the last lecture we will look beyond the Standard Model at which time we will develop whatever formalism we need. The goal of this section is not to be complete or detailed – but merely to build a foundation from which we can extract useful experimental tests at the Z^0 .

The Standard Model is characterized by the gauge group

$$SU(3)_{\text{color}} \wedge SU(2) \wedge U(1)\ .$$

Leptons are pointlike particles which couple to the gauge bosons of $SU(2)$ through their weak charge and to the photon of $U(1)$ through their electric charge. There are six leptons e, μ, τ, and their zero mass partners ν_e, ν_μ, and ν_τ. There are six quarks u, d, s, c, b and t which carry color and there are three color states for each quark. Leptons have no color charge and are therefore "blind" to the strong interaction.

The left handed fermions are arranged in doublets:

$$\begin{pmatrix}\nu_e\\ e\end{pmatrix}_L \quad \begin{pmatrix}\nu_\mu\\ \mu\end{pmatrix}_L \quad \begin{pmatrix}\nu_\tau\\ \tau\end{pmatrix}_L \qquad \begin{matrix}T_3 = 1/2\\ -1/2\end{matrix}$$

$$\begin{pmatrix}u\\ d'\end{pmatrix}_L \quad \begin{pmatrix}c\\ s'\end{pmatrix}_L \quad \begin{pmatrix}t\\ b'\end{pmatrix}_L \qquad \begin{matrix}T_3 = 1/2\\ -1/2\end{matrix}$$

where T_3 is the $3rd$ component of the weak charge. The primes on the quarks indicate that flavor conservation in the quark sector is not perfect. This generation mixing can be summarized by the elements of the Kobayashi–Maskawa matrix – the most familiar component being the Cabibbo angle which tells us that the d quark has a $\sim 5\%$ strange quark admixture. More succinctly – in the quark sector the weak eigenstates are related by a rotation matrix to the mass eigenstates. There are no analogous flavor changing currents in the neutral sector.

Right handed fermions appear in singlets, u_R, d_R $\ldots t_R$, e_R, μ_R, τ_R and, since the ν's are massless, there are no right handed ν's. $T_3 = 0$ for all right handed fermions.

There are nine massless bosons in the standard model – 8 gluons and the photon. There are 3 massive vector bosons W^+, W^- and Z^0 and in the minimal model with one Higgs doublet there is one neutral scalar, H^0 . Gluons carry color (unlike photons which don't carry charge) and hence $SU(3)_{\text{color}}$ is non-abelian. Since gluons carry color they can couple to other gluons. The polarization of the QCD vacuum by virtual quark and gluon pairs results in an anti-screening of color charge. This can be contrasted with the screening of electric charge by virtual e^+e^- pairs in QED. This anti–screening leads to the notion of confinement of quarks and the decrease of the strong coupling constant α_s, with increasing q^2. Free quarks should not be seen and this notion will be tested at the Z^0 although not discussed further in these lectures.

The Standard Model does not predict masses for the fundamental particles. The $W^\pm$, Z^0 masses are given in terms of the parameters $\sin^2\theta_W$:

$$M_W^2 = \frac{\pi\alpha}{\sqrt{2}G_F}\,\sin^2\theta_W$$

$$M_{Z^0}^2 = \frac{M_W^2}{\cos^2\theta_W}$$

where α is the fine structure constant and G_F is the Fermi coupling constant. The H^0 mass is expected to fall in the range $7.5 \lesssim M_{H^0} \lesssim 10^3$ TeV. This however is of no consolation to the experimentalist searching for the H^0 .

The electroweak interactions of all the gauge fields are determined by e, the electric charge, and one free parameter θ_W. Spinors couple to the photon field with strength e and to the Z^0 with strength

$$-e/\sin\theta_W\cos\theta_W\left(T_3^{R/L}-Q\sin^2\theta_W\right)=2\sqrt{2}\left(\frac{M_Z^2G_F}{\sqrt{2}}\right)^{1/2}\left(T_3^{R/L}-Q\sin^2\theta_W\right)$$

where R/L indicates left and right couplings and Q is the charge of the fermion.

We can now write down that piece of the electroweak neutral lagrangian which is of interest to us in these lectures:

a) for leptons (characterized by e, ν)

$$\mathcal{L}_{0-e}=e\,\bar{e}\,\gamma^\mu\,e\,A_\mu-\frac{1}{\sqrt{2}}\left(\frac{G_FM_Z^2}{\sqrt{2}}\right)^{1/2}\bar{\nu}\,\gamma^\mu(1-\gamma_5)\nu\,Z_\mu$$

$$-\frac{1}{\sqrt{2}}\left(\frac{G_FM_Z^2}{\sqrt{2}}\right)^{1/2}[2x_W\,\bar{e}\,\gamma^\mu(1+\gamma_5)e\,Z_\mu+(2x_W-1)\bar{e}(1-\gamma_5)e\,Z_\mu]$$

where

$$x_W=\sin^2\theta_W$$

and b) for quarks with charge Q, weak isospin T

$$\mathcal{L}_{0-q}=Q\,\bar{q}\,\gamma^\mu\,q\,A_\mu-\frac{1}{\sqrt{2}}\left(\frac{G_FM_Z^2}{\sqrt{2}}\right)^{1/2}\bar{q}\,\gamma^\mu[(1+\gamma_5)T_3-2x_WQ]q\,Z_\mu\ .$$

A more complete derivation and discussion can be found in reference 8 chapters 6 and 7. In figure 9 we give all the Feynman rules required for these lectures. Figure 9 (a) follows from the Lagrangian above, while the derivation of the rules in figure 9 (b) is given by Quigg in reference 8.

We are now in a position to calculate the basic process for $e^+e^-\to\gamma$, $Z^0\to f\bar{f}$ as shown in figure 10. The matrix element M is given by

$$M(e^+e^-\to\gamma,Z^0\to f\bar{f})=$$

$$-ie^2\bar{u}(f,q^-)\gamma_\lambda Q_f v(f,q^+)\frac{g^{\lambda\nu}}{S}\bar{v}(e,p^+)\gamma_\nu u(e,p^-)$$

$$+i/2\left(\frac{G_FM_Z^2}{\sqrt{2}}\right)\bar{u}(f,q^-)\gamma_\lambda[R_f(1+\gamma_5)+L_f(1-\gamma_5)]v(f,q^+)$$

$$\times\frac{g^{\lambda\nu}}{S-M_Z^2}\,v(e,p^+)\gamma_\nu[R_e(1+\gamma_5)+L_e(1-\gamma_5)]u(e,p^-)\ .$$

This matrix element is applicable to all $f\bar{f}$ final states except e^+e^- where there

is, in addition, a t channel contribution. The quantities L and R are defined in figure 9. Now some kinematics. Assume $S(=4E^2_{\rm beam})$ is much larger than the electron and fermion masses, then

$$p^+ = E_{\rm beam}(1,0,0,1)$$

$$p^- = E_{\rm beam}(1,0,0,-1)$$

$$q^+ = E_{\rm beam}(1,\sin\theta,0,\cos\theta)$$

$$q^- = E_{\rm beam}(1,\sin\theta,0,-\cos\theta)$$

where $\cos\theta$ is the polar angle of the fermion relative to the incoming electron. So

$$p^+p^- = E^2_{c.m.}/2 = S/2 = q^+q^-$$

$$p^+q^+ = 1/4\ S(1-\cos\theta) = p^-q^-$$

$$p^+q^- = 1/4\ S(1+\cos\theta) = p^-q^+ \quad .$$

We now average over all initial spins, sum over all final spins to obtain a differential cross section

$$\begin{aligned}\frac{d\sigma}{dz} = \frac{|M|^2}{32\pi S} &= \frac{\pi\alpha^2 Q_f^2 D}{2S}(1+z^2) \\ &+ \frac{\alpha Q_f D G_F M_z^2(S-M_z^2)}{8\sqrt{2}[(S-M_z^2)+M_z^2\Gamma_z^2]} \\ &\quad [(R_e+L_e)(R_q+L_q)(1+z^2)+2(R_e-L_e)(R_q-L_q)z] \\ &+ \frac{D G_F M_z^4 S}{64\pi[(S-M_z^2)+M_z^2\Gamma_z^2]} \\ &\quad [(R_e^2+L_e^2)(R_q^2+L_q^2)(1+z^2)+2(R_e^2-L_e^2)(R_q^2-L_q^2)z]\end{aligned} \tag{4}$$

where $z=\cos\theta$ and we have replaced the Z^0 propagator with the formula for an unstable resonance with width Γ. The number D is to take into account color degrees of freedom. For $f \equiv$ quark, $D=3$, otherwise $D=1$. The three terms in the cross section are the purely electromagnetic contribution, the interference between the weak and electromagnetic diagrams and the purely weak contribution. Notice that a) the interference term disappears at $\sqrt{S}=M_Z$ as it should b) the first term is just the point QED differential cross section and c) at $\sqrt{S}=M_Z$ the purely weak term dominates. Since we are interested in physics at the Z^0 , we set $\sqrt{S}=M_Z$ and change notation to

axial coupling: $2a = (L - R)$

and vector coupling: $2v = (L + R)$.

Hence $L = a + v$, $R = v - a$, $L^2 + R^2 = 2(a^2 + v^2)$ and $L^2 - R^2 = 2av$ and we find at $\sqrt{S} = M_Z$

$$\frac{d\sigma_{ff}}{dZ} = \frac{DG_F^2 M_Z^4}{16\pi\Gamma_Z^2}\left[(a_e^2 + v_e^2)(a_f^2 + v_f^2)(1 + \cos^2\theta) + 2a_e v_e a_f v_f \cos\theta\right] \quad . \tag{5}$$

It is useful to tabulate the couplings and the sum of their squares:

$$\begin{aligned} v_f &= T_3^f - 2Q_f \sin^2\theta_W \\ a_f &= T_3^f \ . \end{aligned} \tag{6}$$

Assuming $\sin^2\theta_W = 0.22$ (which we will do throughout for convenience) we find the values in Table I.

TABLE I

	Q	T_3	a	v	$a^2 + v^2$
e, μ, τ	-1	-1/2	-1/2	-.06	.2536
ν_e, ν_μ, ν_τ	0	1/2	1/2	1/2	1/2
d, s, b	-1/3	-1/2	-1/2	-.35	.375
u, c, t	+2/3	+1/2	1/2	.21	.29

We turn our attention back to equation 5. The term linear in $\cos\theta$ contributes a front-back asymmetry, A_{F-B}. $A_{F-B} \propto v_e\, v_f$ which, for charged leptons, is a very small number. However a measurement of A_{F-B} for charged leptons has great sensitivity to $\sin^2\theta$ as we will see later in this section. Since $\int_0^\pi \cos\theta d\theta = 0$ the term linear in $\cos\theta$ does not contribute to the total cross section.

Integrating the term in $(1+\cos^2\theta)$ yields the total cross section for producing a final state $f\bar{f}$ at the Z^0 :

$$\sigma_{ff} = \frac{DG_F^2 M_Z^4}{6\pi\Gamma_Z^2}(v_e^2 + a_e^2)(v_f^2 + a_f^2) \ .$$

We omit here the derivation of Γ_Z (see reference 8) but note that

$$\Gamma_Z = \frac{G_F M_Z^3}{24\sqrt{2}\pi} \sum_i (v_i^2 + a_i^2) D_i \tag{7}$$

where i ranges over all fundamental fermions and D_i is the color factor (3 for

quarks, 1 for leptons). Notice this formula is analogous to that for

$$R = \frac{\sigma_{\text{hadrons}}}{\sigma_{\text{point}}} = \sum_i Q_i^2 D_i \ .$$

Referring to equations 6 and 7 and assuming 6 quarks and ignoring the t quark mass (we discuss its effect later) one finds

$$\Gamma_Z = \frac{G_F M_Z^3 \sqrt{2}}{\pi}(1 - 2x_W + \frac{8}{3}\, x_W^2) \ .$$

We can obtain σ_{point}, which is the lepton point QED cross section, from the first term in equation 4:

$$\sigma_{\text{point}} = \frac{\pi\alpha^2}{2S} \int (1 + \cos^2\theta) d\cos\theta$$

$$= \frac{4\pi\alpha^2}{3S}$$

$$\simeq \frac{87 nb^{-1}}{S} \ .$$

Hence we can write

$$R_{ff} = \frac{\sigma_{ff}}{\sigma_{\text{point}}} = \frac{D(a_f^2 + v_f^2)(a_e^2 + v_e^2)}{16\alpha^2(1 - 2x_W + 8x_W^2/3)^2} \ . \qquad (8)$$

Assuming 6 quarks, ignoring the finite t mass and setting $\sin^2\theta_W = .22$ one finds at the Z^0 the R values in Table II. Also shown in Table II are the branching fraction for each process. Hence under these assumptions $R_{Z^0} \approx 5200$ and $B(Z^0 \rightarrow \text{hadrons}) \simeq 72\%$. This value of R_{Z^0} has not been corrected for initial state radiation effects which has the effect of lowering the peak cross section with a compensating "radiative tail" on the high side of the resonance. These radiative effects are discussed more fully in reference 9 – we quote here the approximate result. For a narrow resonance with peak cross section σ_0 the actual cross section, after the inclusion of radiative effects, is

$$\sigma_{\text{peak}} \approx \left(\frac{\Gamma}{m}\right)^t \sigma_0 + \left(\delta_0 + \frac{13}{2} t\right) \sigma_0$$

where $t = 2\alpha/\pi\ (\ell n\ S/m_e^2 - 1)$ is the so called equivalent radiator and $\delta_0 = 2\alpha/\pi\ (\pi^2/6 - 17/36) \simeq 0.005$. At $\sqrt{S} = M_Z$, $t = .11$ and

$$\sigma_{\text{peak}} \approx 0.8\sigma_\sigma \ .$$

Hence the radiatively corrected R is approximately 4200 on the Z^0 .

TABLE II

CHANNEL $(f\bar{f})$	R_{ff}	Γ_{ff}/Γ_{Z^0} (%)
each $\nu\bar{\nu}$	313	6.1
$\mu^+\mu^-$, $\tau^+\tau^-$, e^+e^{-*}	159	3.1
$u\bar{u}$, $c\bar{c}$, $t\bar{t}$	550	10.6
$d\bar{d}$, $s\bar{s}$, $b\bar{b}$	704	13.6

* We have ignored t channel diagrams which are only important at small values of θ.

We return now to the problem of how to incorporate the effects of large masses ($\omega rt\ \sqrt{S}$) for the final state fermion in equation 4. In a general way we can write

$$\frac{d\sigma_{f\bar{f}}}{d\theta} = f(\beta_f, \theta)\ \sigma(m_f = 0)$$

and

$$\sigma_{f\bar{f}} = f(\beta_f)\sigma(m_f = 0)$$

where β_f is the fermion velocity and m_f is the fermion mass. For vector couplings

$$f(\beta_f, \theta) = \frac{3}{16\pi}\beta_f[(1 + \cos^2\theta) + (1 - \beta_f^2)\sin^2\theta]$$

and

$$f(\beta_f) = 1/2\ \beta_f(3 - \beta_f^2)\ .$$

For axial - vector couplings

$$f(\beta_f, \theta) = \frac{3}{16\pi}\beta_f^3(1 + \cos^2\theta)$$

and

$$f(\beta_f) = \beta_f^3\ .$$

Therefore for the t quark with velocity β_t, the correct form of the contribution to the Z^0 width is (see equation 7)

$$\Gamma(Z^0 \to t\bar{t}) = \frac{G_F M_Z^3}{8\sqrt{2}\pi}(v_t^2\ \frac{1}{2}\beta_t(3 - \beta_t^2) + a_t^2\beta_t^3)\ .$$

Figure 11 shows the suppression of $t\bar{t}$ relative to a full strength (light) charge two-thirds quark as a function of the t quark mass. Since we know from PETRA

that $M_t \gtrsim 23$ GeV/c^2 the $t\bar{t}$ final state at the Z^0 is suppressed at least to 0.7 of the $u\bar{u}$ rate.

We return now to the forward backward charge asymmetry (A_{F-B}) discussed earlier. Consider for the moment the concrete example of the final state $\mu^+\mu^-$ as applied to our master formula (4). We will get a contribution to A^{μ}_{F-B} from terms linear in $z = \cos\theta$.

$$A^{\mu}_{F-B} = \frac{\int_0^1 \frac{d\sigma}{dz}dz - \int_{-1}^0 \frac{d\sigma}{dz}dz}{\int_0^1 \frac{d\sigma}{dz}dz + \int_{-1}^0 \frac{d\sigma}{dz}dz} = \frac{N^F_{\mu^-} - N^B_{\mu^-}}{N^F_{\mu^-} + N^B_{\mu^-}}$$

where $N^F_{\mu^-}(N^B_{\mu^-})$ is the number of μ^- in the forward (backward) hemisphere relative to the incoming e^- direction. Consider now two limiting cases:

a) $S \ll M_Z^2$

$$A^{\mu}_{F-B} \simeq \frac{3G_F}{4\alpha\sqrt{2}\pi} \frac{S}{(1 - S/M_Z^2)} a_e \left(\frac{a_\mu}{Q_\mu}\right)$$

We notice that 1) A^{μ}_{F-B} grows like $E^2_{\text{c.m.}}$, 2) is independent of the vector couplings and hence insensitive to $\sin^2\theta_W$, 3) has very mild sensitivity to M_Z and 4) is negative.

b) $S = M_Z^2$

$$A^{\mu}_{F-B} = \frac{3a_e a_\mu v_e v_\mu}{(v_e^2 + a_e^2)(v_\mu^2 + a_\mu^2)} \simeq 4.3\% \qquad (9)$$

The character of the asymmetry on the Z^0 is quite different than at lower energies. A^{μ}_{F-B} is now positive and proportional to $v_e v_\mu$ which makes it small but very sensitive to $\sin^2\theta_W$. Hence we can sketch out the behavior of A^{μ}_{F-B} as shown in figure 12. Referring back to equation 6 we find at the Z^0

$$A^{\mu}_{F-B} = \frac{3(1 - 4x_W)^2}{4(1 - 4x_W + 8x_W^2)^2}\ ,\ x_W = \sin^2\theta_W$$

and

$$\frac{1}{15}\frac{dA^{\mu}_{F-B}}{A^{\mu}_{F-B}} \simeq \frac{d\sin^2\theta}{\sin^2\theta}\ . \qquad (10)$$

Hence the statement that a measurement of A^{μ}_{F-B} provides substantial sensitivity to $\sin^2\theta_W$.

From equations 8 and 9 applied to $e^+e^- \to Z^0 \to e^+e^-$ one finds

$$A^e_{F-B} = \frac{3a_e^2 v_e^2}{(a_e^2 + v_e^2)^2}$$

and

$$R^{e^-e^+} \propto (v_e^2 + a_e^2)^2 \, .$$

From these two equations one can determine a_e and v_e but not their relative signs. Is it possible to measure the relative sign? The answer is yes, as long as one can measure the fermion polarization of one of the charged $f\bar{f}$ final states. It turns out that the only practical final state for a polarization measurement is $\tau^+\tau^-$. Since parity is violated in the neutral current interaction, even in the absence of $e^\pm$ beam polarization, the Z^0 is produced polarized as are its decay products. The polarization P is given by

$$\begin{aligned} P^{f\bar{f}} &= \frac{\sigma_R - \sigma_L}{\sigma_R + \sigma_L} \\ &= (R_f^2 - L_f^2)/(R_L^2 + L_f^2) \\ &= -\frac{2a_f v_f}{(a_f^2 + v_f^2)} \, . \end{aligned}$$

Now the ratio

$$A^f_{F-B}/P^{f\bar{f}} = -3a_e v_e/(a_e^2 + v_e^2)$$

is independent of the final state fermion couplings and measures directly the relative sign of v_e and a_e. By measuring $R^{e^+e^-}$, A^e_{F-B} and the τ polarization one finds a_e and v_e. Then from $R^{\mu^+\mu^-}$, A^μ_{F-B}, $R^{\tau^+\tau^-}$, A^τ_{F-B} one can obtain the μ and τ axial and vector couplings. In this way the universality of the weak interactions is checked. In addition each measurement of a vector coupling provides a measurement of $\sin^2\theta_W$.

This ends our discussion of the Standard Model and the theoretical expectations. We now turn our attention to the experimental measurements.

5. EXPERIMENTAL TESTS OF THE STANDARD MODEL AT THE Z^0

5.1 CHARGED LEPTON COUPLINGS AND $\sin^2\theta_W$

We have just outlined above a program for measuring the charged lepton couplings and $\sin^2\theta_W$. To do this we must isolate events of the type $Z^0 \to e^+e^-$, $\mu^+\mu^-$ and $\tau^+\tau^-$. This is a rather simple experimental task and is routinely done at PEP and PETRA. The experimental problems are even easier at the Z^0 . For the e^+e^- and $\mu^+\mu^-$ final states one requires two opposite sign, charged particles which are "back-to-back" and carry the full beam energy. Electrons are trivially distinguished from muons using a rudimentary electromagnetic shower counter. To measure that the tracks have opposite sign requires only a modest momentum precision of $\sigma_p/p^2 \approx 1\%$ - all the LEP and SLC detectors will do far better than this. These channels have high rates ($B(Z^0 \to \ell^+\ell^-) = 3\%$) and there are no background problems. To identify the $\tau^+\tau^-$ final state one will require a topology in which the one τ decays to a single charged prong ($B(\tau \to 1$ charged prong $= 84\%$)) and the other τ decays to three charged prongs and any number of neutrals ($B(\tau \to 3$ charged prongs $= 16\%$)). This gives a very clean $\tau^+\tau^-$ sample at a rate of $3\% \times(2 \times 0.84 \times 0.16) \approx 1\%$. Hence the $\tau^+\tau^-$ final state will contribute information with a statistical weight of $\approx \sqrt{3}$ less than $\mu^+\mu^-$ or e^+e^-.

Consider now our canonical 10^6 produced Z^0's which will provide 30,000 $\mu^+\mu^-$ events. The asymmetry measurement will suffer a statistical error of $(\sqrt{30,000})^{-1} \simeq .005$. Hence (see equations 9 and 10)

$$\frac{\delta A}{A} = \frac{.005}{.043} = .12$$

and

$$\frac{\delta(\sin^2\theta)}{\sin^2\theta} = \frac{1}{15}(.12) = .008\ .$$

Assuming $\sin^2\theta_W = 0.22$, $\delta(\sin^2\theta_W) = .0017$! (Notice this is about an order of magnitude better than measurements from ν interactions or the polarized e^-d experiment.) The measurement error for the coupling constants is obtained after laborious propagation of errors which we omit here but are found in reference 6b) page 28:

$$\delta(v/a) \simeq 0.008 \quad \text{for} \quad e^+e^-,\ \mu^+\mu^-\ .$$

The measurements for the $\tau^+\tau^-$ channel will be less precise by about $\sqrt{3}$ as discussed above.

The measurement of R^{ee}, $R^{\mu\mu}$ and $R^{\tau\tau}$ amounts to counting the number of events in each category, making a correction for inefficiencies and normalizing to the luminosity. Typically these measurements can be done to $\approx 3\%$, the main limitation arising from the normalization. As we mentioned in the previous section the final ingredient needed to measure the couplings is the measurement of the τ polarization. This is best done using the decay $\tau \to \pi\nu$ although the leptonic decays $\tau \to e\nu\nu$ and $\tau \to \mu\nu\nu$ are also useful. With modest particle identification the different τ modes can be identified. The measurable sensitive to the τ polarization is the $\pi^{\pm}$ or $\ell^{\pm}$ momentum spectrum. For a τ of polarization P_τ the fractional momentum of the π in the decay $\tau \to \pi\nu$ is given by[10]

$$\frac{dN_\pi}{dx_\pi} = 1 + P_\tau(2x_\pi - 1)$$

where $x_\pi = 2E_\pi/E_{c.m.}$. The average value of x_π is

$$\langle x_\pi \rangle = (3 + P_\tau)/6$$

and hence a measurement of $\langle x_\pi \rangle$ yields P_τ. Likewise[10] for $\tau \to \ell\nu\bar{\nu}$.

$$\frac{dN_\ell}{dx_\ell} = \frac{1}{3}[5 - 9x_\ell^2 + 4x_\ell^3 + P_\tau(1 - 9x_\ell^2 + 8_\ell^3)]$$

and

$$\langle x_\ell \rangle = (7 - P_\tau)/20 \, .$$

So for the $\tau \to \pi\nu$ measurement we can select two prong and four prong events as shown in figure 13. One must now ensure that the single π's are indeed π's. This involves making sure that the track is neither a muon nor an electron. The separation of pions from muons and electrons in such a low multiplicity environment is easy particularly for momenta above 1 GeV/c. All the LEP and SLC detectors will be able to make a good separation. In addition making a good determination of $\langle x \rangle$ requires a momentum precision of $d\sigma_p/p^2 \lesssim 0.5\%$. The experimental details of the measurement are discussed in great detail in reference 6b) page 103 and we will borrow liberally from that discussion. We should remind ourselves that $P_\tau = -2a_\tau v_\tau/(a_\tau^2 + v_\tau^2) = f(\sin^2\theta_W)$ so that a measurement of P_τ is also a measurement of $\sin^2\theta_W$. In particular if $\sin^2\theta_W = 1/4$, $P_\tau \equiv 0$. Figure 14 shows the predicted dN/dx spectra for different values of $\sin^2\theta_W$. The simulation discussed in reference 6b) used 10^6 Z^0's and a detector with parameters similar to the typical SLC/LEP detector. Figure 15 shows the simulated experimental momentum spectra for the decay pion and lepton where $\sin^2\theta_W$ has been set to 0.23. From these spectra the average values obtained

are

$$\langle x_\pi \rangle = 0.483 \pm 0.006$$

$$\langle x_\ell \rangle = 0.359 \pm 0.003 \ .$$

The solid lines on the figure correspond to the theoretical curves from figure 14 and demonstrate how the finite momentum resolution ($\sigma_p/p^2 = 0.5\%$ for this simulation) distorts the high x end of the spectrum.

For the decay channel $\tau \rightarrow \pi\nu$, $P_\tau = 6\langle x \rangle - 3$ and therefore from this simulation

$$P_\tau \approx 0.11$$

$$\delta P_\tau = 6\delta\langle x \rangle = 0.036 \ .$$

Also from the previous discussion we have

$$A^\tau_{F-B} \approx 0.043 \pm 0.008 \ .$$

We obtain the relative sign of a_e and v_e from the ratio

$$\frac{A^\tau_{F-B}}{P_\tau} = -\frac{3a_e v_e}{(a_e^2 + v_e^2)} \ .$$

Clearly our ability to tell the relative sign is limited by the P_τ measurement and hence for this toy experiment one would determine the relative sign of v_e and a_e to $\gtrsim 3\sigma$ from the decay $\tau \rightarrow \pi\nu$. Additional statistical power would come from the decay modes $\tau \rightarrow e\nu\bar{\nu}$ and $\tau \rightarrow \mu\nu\bar{\nu}$. As a by-product one gets a measurement of $\sin^2\theta_W$. A little bit of math yields

$$\frac{dP_\tau}{P_\tau} \approx 95 \ d(\sin^2\theta_W)$$

and hence

$$\delta(\sin^2\theta_W) \approx 0.004 \quad \text{from} \quad \tau \rightarrow \pi\nu$$

$$\delta(\sin^2\theta_W) \approx 0.007 \quad \text{from} \quad \tau \rightarrow \ell\nu\bar{\nu} \ .$$

Now life becomes much easier if one has a longitudinally polarized electron (or positron) beam. As we discussed in section 2, the SLC is expected to have a longitudinally polarized e^- beam with polarization $P_{e^-} \gtrsim 50\%$. In addition, on a pulse by pulse basis, the sign of the polarization can be switched from left to right. Now one can do a very simple experiment namely to measure the total cross section for left polarized electrons (σ_L) and that for right polarized

electrons (σ_R). These cross sections will not be equal and we can form an asymmetry

$$A_{L-R} = \frac{\sigma_L - \sigma_R}{\sigma_L + \sigma_R} = -2P_{e^-} \frac{a_e v_e}{(a_e^2 + v_e^2)} .$$

Recognize that A_{L-R} immediately gives the relative sign of v_e and a_e thus obviating the need for the τ polarization measurement. In addition this is a very simple experiment to perform and unlike the measurement of A_{F-B}, all the Z^0 decay (except $Z^0 \to \nu\bar{\nu}$ of course) events can be used and statistics are no problem at all. For $P_{e^-} = 0.5$ and $\sin^2\theta_W = 0.22$, $A_{L-R} = 12\%$ – three times larger than A^{μ}_{F-B}. So it will be much easier to measure A_{L-R} on the Z^0 peak than A^{f}_{F-B}.

The error in A_{L-R} is dominated by the measurement error in P_{e^-}. How do we measure P_{e^-}? The idea is to use Möller scattering ($e^-e^- \to e^-e^-$) by intercepting the e^- beam after the collision point with a thin magnetized foil. The precision is predicted to be $\delta P_{e^-}/P_{e^-} \lesssim 5\%$. The method is more fully discussed in Ref. 6b) page 11. Clearly

$$\frac{\delta A_{L-R}}{A_{L-R}} = \frac{\delta P_{e^-}}{P_{e^-}} = 0.05 .$$

Also

$$\frac{\delta A_{L-R}}{A_{L-R}} \approx \frac{7.3\delta(\sin^2\theta_W)}{\sin^2\theta_W}$$

and hence $\delta(\sin^2\theta_W) \approx 0.0015$. How long would we need to run? Long enough so that the statistical error is small compared with 5%. 10^5 Z^0's would be fine – this is about 20 days at good machine performance. Notice that comparable precision in $\sin^2\theta_W$ is obtained from A^{μ}_{F-B} and A_{L-R}, but the running time is 10 times less using A_{L-R}. In addition the relative sign of a_e and v_e is measured quickly and without using a measurement of the τ polarization. One sees that it is most desirable to have a polarized electron beam at the Z^0 factories.

5.2 What Do We Learn From the Z^0 Mass?

The ability to measure M_{Z^0} and Γ_{Z^0} will be determined less by the detector than the intrinsic stability of the machines and knowledge of radiative corrections. The intrinsic precision of the machine is excellent namely $\delta E/E \approx 0.1\% \Rightarrow \delta M_{Z^0} \simeq 100$ MeV.

The standard model prediction can be tested then using

$$M_{Z^0} = \left(\frac{\pi\alpha}{\sqrt{2}G_F}\right)^{1/2} \frac{1}{\sin\theta_W \cos\theta_W}$$

where θ_W is measured in Z^0 decay. Of course $\sin^2\theta_W$ has been measured in

low energy experiments, but we cannot use this in the formula above because of weak radiative corrections of the type shown in figure 16. The bare mixing angle of the theory is $\sin^2\theta_W^0 = e^2/g^2$ where e and g are the $U(1)$ and $SU(2)$ coupling constants. The renormalized $\sin^2\theta_W^R$ is related to $\sin^2\theta_W^0$ by a radiative expansion:

$$\sin^2\theta_W^0 = \sin^2\theta_W^R(1 - \alpha/\pi f(\sin^2\theta_W) + O(\alpha^2)\ldots) .$$

This is more carefully discussed in reference 11 and was discussed at this Summer School by Maiani. Estimates are that $\sin^2\theta_W$ is roughly 7% larger at the Z^0 than the measurements at lower energies or

$$M_{Z^0} = \left(\frac{\pi\alpha}{\sqrt{2}G_F}\right)^{-1/2} \frac{1 + 0.035}{\sin\theta_W\cos\theta_W}$$

$$= \frac{37.28(1.035)}{\sin^2\theta_W\cos\theta_W}$$

Also

$$\frac{dM_Z}{M_Z} = -\frac{(1 - 2\sin^2\theta_W)}{2\cos^2\theta_W}\frac{d\sin^2\theta_W}{\sin^2\theta_W}$$

$$\simeq -0.36\,\frac{d\sin^2\theta_W}{\sin^2\theta_W} .$$

Now if we trust the radiative correction calculation then $\delta M_Z = 100$ MeV $\Rightarrow$ $\delta(\sin^2\theta_W) = 0.0007$! However it is unlikely that the machine performance, especially in the early days will yield such a small error in $E_{c.m.}$.

If on the other hand we don't trust the radiative correction calculations at all and attribute the error in M_{Z^0} entirely to the radiative correction then $\delta M_Z/M_Z = 3.5\%$ $\Rightarrow$ $\delta(\sin^2\theta_W) = 0.023$ which is of course an uninteresting result. The real importance of the measurement of M_{Z^0} will probably be to check the radiative correction calculations using as input for θ_W measurements at the Z^0 from say the couplings or asymmetries.

5.3 The Measurement of the Z^0 Width

The Z^0 width is given by (see section 3)

$$\Gamma_{Z^0} = \frac{G_F M_Z^3}{24\sqrt{2}\pi}\sum_f (v_f^2 + a_f^2)(1 + \delta_f)$$

where f ranges over all flavors and colors and δ_f accounts for the effect of final state radiation either off an electric charge or a color charge. Contributions to

the final state radiative corrections are shown in figure 17 and

$$\delta_f \approx \frac{3}{4}\frac{\alpha Q_f^2}{\pi} + \frac{\alpha_s S}{\pi} D_f$$

where Q_f is the fermion electric charge and $D_f = 0, 1$ for leptons, quarks. The first term ($\leq 0.17\%$) arises from photon emissions and can be ignored while the second term, familiar to us as the QCD correction to $R = \sigma_{\text{hadrons}}/\sigma_{\text{point}}$, represents a correction to Γ_{Z^0} of about 4%. We will see later in this section that all the QCD apparatus and calculations done for continuum e^+e^- interactions are equally valid at the Z^0 and hence the familiar QCD radiative correction term α_s/π.

If we assume 5 quarks (no t for the moment) and 6 leptons one finds for $\sin^2\theta_W = 0.22$ (see Table I)

$$\Gamma_{Z^0} = 0.088[3 \times 1.01 + 3 \times 2.0 + 3 \times 3 \times 1.04 \times 1.5 + 3 \times 2 \times 1.04 \times 1.17]$$

$$= 2.67 \text{ GeV} \ .$$

Suppose we measure Γ_{Z^0} directly and want to compare with the above Standard Model prediction. What are the uncertainties in this prediction? If we know α_s (Z^0) to 20%, the radiative correction term contributes an uncertainty of 0.8%. If we know M_Z to 0.1%, we get an uncertainty in Γ_{Z^0} of 0.3%. If $\sin^2\theta_W$ is known to 0.005 say then this translates into an uncertainty of $\simeq 0.5\%$ in Γ_{Z^0}. So the inherent errors in the Standard Model prediction should be small $\lesssim 1\%$. However we could run into some systematic problems associated with poor machine performance or initial state radiative effects.

A less direct but probably simpler method to measure the Z^0 width is via σ_{ff}. Recall for a $f\bar{f}$ final state

$$\sigma_{ff} = \frac{DG_F^2 M_Z^4}{6\pi\Gamma_Z^2}(v_e^2 + a_e^2)(v_f^2 + a_f^2) \ .$$

Consider the $\mu^+\mu^-$ final state:

$$\frac{d\sigma_{\mu\mu}}{\sigma_{\mu\mu}} = 2\frac{d\Gamma_Z}{\Gamma_Z} \approx -0.22\,\frac{d\sin^2\theta_W}{\sin^2\theta_W}$$

Hence if $\delta(\sin^2\theta_W) \approx 0.005$, $\delta\Gamma_Z \approx 0.1\%$! The major experimental problem is measuring the luminosity which can safely be done to $\lesssim 5\%$. This would yield a measurement of Γ_{Z^0} with an error $\delta\Gamma_{Z^0} \simeq 70$ MeV. This error can be calibrated by recalling that $\Gamma(Z^0 \to \nu\bar{\nu}) \simeq 170$ MeV. So this method of measuring σ_{ff} looks very promising.

Suppose we measure Γ_{Z^0} and it is larger than the prediction of the Standard Model. What have we learned? Or more precisely how do we tell what is contributing to the additional width. Any weakly coupled object with mass $\lesssim M_{Z^0}/2$ will contribute to the Z^0 width. This could be a new quark, new heavy lepton, SUSY particles, . . .

We could tell if the extra width was coming from $Z^0 \rightarrow$ hadrons by measuring the quantity

$$R' = \frac{\sigma_{\text{hadrons}}}{\sigma_{\mu\mu}}$$

$$= 3(1+\alpha_s/\pi)\sum_q (a_q^2+v_q^2)/(a_\mu^2+v_\mu^2)\ .$$

For 5 flavors, $R' = 20.8$. The error in measuring R' will be about 5% or $\delta R' \approx 1$. Could we find the t quark using R'? We can calculate R'_t remembering to account for its finite mass:

$$R'_t = \frac{3(a_t^2\beta^3 + v_t^2\beta(3-\beta^2)/2)(1+\alpha_s/\pi)}{(v_\mu^2+a_\mu^2)}$$

$$= 3\beta[0.92\beta^2+0.26] \qquad \text{for} \qquad \sin^2\theta_W = 0.22\ .$$

For $M_t = 30$, 35 and 40 GeV/c^2, $R'_t = 1.8$, 1.3 and 0.8. Hence for $M_t \gtrsim 30$ GeV/c^2, R' is not a sensitive way to find the t quark. There are much easier methods involving event shapes and event topologies and we turn our attention to them now. We return later to the question of how to understand a larger than expected Γ_{Z^0}

5.4 Searching for the Top Quark

We saw above that the large t mass made it difficult to search for the t quark using R'. However we can devise t quark search procedures which are increasingly successful as M_t gets larger. Naturally as $M_t \rightarrow M_{Z^0}/2$ we get a rapidly decreasing yield of $Z^0 \rightarrow t\bar{t}$ events as discussed in section 2.

Suppose we ran for a week at SLC or LEP with a modest average machine luminosity of $3\times10^{29}\ cm^{-2}\ sec^{-1}$. We collect hadronic events and do a sphericity shape analysis[12] on the events. Hadronic events are very simple to isolate because of their high multiplicity and large detected energy. They will be isolated with high efficiency and no background. The sphericity analysis will provide three orthogonal axes, two of which define a plane – the event plane – which is the plane which contains most of the momentum of the detected particles. The aplanarity is a measure of the momentum out of the event plane. Because transverse momentum (P_t) is limited in the fragmentation process and because the 5

known quarks will all have high velocities in Z^0 decay, the events containing the 5 known quarks will have small aplanarity. However if a heavy quark is produced which has a low velocity, the same limited P_t will result in a considerably larger aplanarity. Figure 18 shows the aplanarity obtained in a simulation of hadronic decays of the Z^0 . The 5 light quarks are shown separately from a 30 GeV/c^2 t quark. A one week run of this type would easily establish the presence of a new heavy quark with $M \gtrsim 25$ GeV/c^2. Presumably this would be the t quark, however it could also be a fourth $q = -1/3$ quark! We will discuss later how to distinguish between these two possibilities experimentally.

Another way to look for heavy quarks is to use the fact that they have copious semileptonic decays. Again because of their heavy mass and low velocity, the leptons arising from such decays make a large angle with respect to the quark (jet) direction. This can be contrasted with leptons arising from the 5 known quarks. Rather than measuring the decay angle, we choose to use the transverse momentum relative to the quark direction (P_t). In an experiment the sphericity (or thrust) axis is a good measure of the $q\bar{q}$ direction and momenta are usually measured relative to this axis. At the Z^0 one can expect to measure the thrust axis to $\lesssim 1°$. Figure 19 shows the result for simulated Z^0 hadronic events in which the P_t^2 of muons has been plotted relative to the quark direction for different parent flavors. The muons (or electrons) coming from the $t\bar{t}$ events (m_t assumed to be 25 GeV/c^2) have substantially larger P_t than the corresponding leptons from the lighter quarks. The P_t spectrum would clearly flag the presence of a new heavy quark. So one has at least two relatively simple, quick ways of looking for the top quark. How would one measure the top quark mass?

The P_t spectrum of the decay leptons would be useful as a rough (3 - 5 GeV/c^2) measure of M_t. This method would rely heavily on the assumptions of the Monte Carlo simulation program, in particular the assumptions needed for t quark fragmentation. Reconstructing the jet mass in the tagged $t\bar{t}$ events does not do a good job either. Figure 20 will illustrate the problem. In figure 20 we see a reconstruction of charged tracks in a $Z^0 \rightarrow d\bar{d} \rightarrow$ hadrons event. The jet axis is clearly defined and an assignment of particles to two quark jets is unambiguous. The jet masses will prove to be useful measureables. But in figure 21 because of the large t mass, it would be very hard to assign the produced particles to two jets in a unique way. Hence a reliable measure of jet mass is impossible.

Probably the best method for determining the t quark mass is to return to figure 11, the t quark threshold curve. If one could find out where one was on the curve, one could "read off" M_t. This method is discussed fully in reference 13.

Recall $\rho = \Gamma_l(\beta)/\Gamma_u$ as plotted in figure 11. Let $r = N_h/N_{\mu\mu}$ where N_h is the number of hadronic events and $N_{\mu\mu}$ is the number of $\mu^+\mu^-$ events. Then

$$\rho = 1 + r\,\frac{\Gamma_{\mu\mu}}{\Gamma_u} - \frac{\Gamma_h}{\Gamma_u}$$

where Γ_h = the hadronic width calculated in the Standard Model for 3 quark generations of massless colored weak isospin doublets. $\Gamma_{\mu\mu}$ and Γ_μ are the partial widths for the $Z^0 \to \mu^+\mu^-$ and $Z^0 \to u\bar{u}$. The experiment is simple – measure r which provides ρ which from figure 11 provides M_t. The measurement of r does not involve a luminosity measurement and should be free of systematics at the 1 - 2 % level. If we assume our canonical $10^6 Z^0$, $N_h \approx 730{,}000$, $N_{\mu^+\mu^-} \approx 31{,}000$ and if $\sin^2\theta_W$ is known to ≈ 0.001 then one obtains a t mass resolution shown in figure 22.

Notice that in order to use this method one requires independent knowledge that $t\bar{t}$ events are being produced at the Z^0 and that there are no other processes which are contributing to N_h.

5.5 Searching for the Neutral Higgs, H^0

At the Bonn Conference in 1981, Okun said[14] that in his mind the outstanding experimental challenge was the search for scalars. He urged experimentalists to "drop everything" and devise cunning searches for the elusive scalars. To date no search has proven successful and it is interesting to speculate how one could search for the H^0 running on the Z^0 .

The H^0 will couple to the heaviest fermions available and this feature will be used in any search for the H^0 . From the Feynman diagram in figure 9 (b) we can calculate the decay rate for the Higgs particle. The matrix element for $H^0 \to f\bar{f}$ is

$$M = -im_f(G_F\sqrt{2})^{1/2}\;\bar{u}(f,p_1)\;v(f,p_2)$$

where m_f is the fermion mass and, in the H^0 rest frame, the fermion momenta are (for $m_f \ll M_{H^0}$)

$$2p_1 = M_{H^0}(1,0,0,1)$$

$$2p_2 = M_{H^0}(1,0,0,-1) \quad .$$

The matrix element squared is given by

$$|M|^2 = m_f^2\sqrt{2}G_F Tr(\not{p}_2\;\not{p}_1)$$

$$= 4m_f^2\sqrt{2}G_F p_1\cdot p_2$$

$$= 2\sqrt{2}G_F m_f^2 M_{H^0}^2 \quad .$$

Therefore

$$\frac{d\Gamma}{d\Omega} = \frac{|M|^2}{64\pi^2 M_{H^0}} = \frac{G_F M_{H^0} m_f^2}{16\pi^2\sqrt{2}} .$$

The decay rate depends on m_f^2 and is isotropic. So if $M_{H^0} < 2M_b$, the H^0 will decay mostly to $c\bar{c}$ and $\tau^+\tau^-$. If $2m_t < M_{H^0} < 2M_b$ then the H^0 will decay mostly to $b\bar{b}$. These conclusions are summarized in figure 23.

How can we search for the H^0? The process $e^+e^- \rightarrow Z^0 \rightarrow H^0H^0$ is forbidden by spin-statistics. The process $Z^0 \rightarrow H^0\gamma$ vanishes in first order because the Z^0 and γ are "orthogonal" – in second order the rate is too small to be of any practical use. The most promising search channel seems to be $Z^0 \rightarrow H^0Z^{0*} \rightarrow H^0\ell^+\ell^-$ (see figure 24) which was first discussed[15] by Bjorken and is also discussed in reference 16. Reference to the Feynman diagrams in figure 9 and a good deal of calculational zeal leads to the relative rate

$$\frac{1}{\Gamma(Z^0 \rightarrow \mu^+\mu^-)} \frac{d\Gamma(Z^0 \rightarrow H^0\ell^+\ell^-)}{dM_{\ell^+\ell^-}} = \frac{\alpha F}{4\pi \sin^2\theta_W \cos^2\theta_W}$$

where

$$F = \frac{10k^2 + 10\lambda^2 + 1 + (k^2 - \lambda^2)[(1 - k^2 - \lambda^2) - 4k^2\lambda^2]^{1/2}}{(1 - k^2)^2}$$

$$M_{\ell^+\ell^-} = \text{lepton pair mass}$$

$$k = M_L/M_{Z^0}$$

and $$\lambda = M_{H^0}/M_{Z^0} .$$

This relative rate, integrated over $M_{\ell^+\ell^-}$, is plotted as a function of M_{H^0} in figure 25. Also shown for comparison is the rate for $Z^0 \rightarrow H^0\gamma$. $B(Z^0 \rightarrow \mu^+\mu^-)$ = 3%, so one sees that for $M_{H^0} \approx 20$ GeV/c^2 $B(Z^0 \rightarrow H^0\ell^+\ell^-) \approx 3 \times 10^{-5}$, a yield of 30 events for 10^6 Z^0 events. Unfortunately the rate drops off very rapidly with increasing H^0 mass and for masses above $\sim$ 40 GeV/c^2 the measurement becomes severely rate limited.

The $H^0\ell^+\ell^-$ signal must be sought in the presence of an enormous background from $Z^0 \rightarrow$ hadrons. For $M_{H^0} \approx 20$ GeV/c^2 there are $\approx 10^4$ $Z^0 \rightarrow$ hadron events per $Z^0 \rightarrow H^0\ell^+\ell^-$ event! Luckily the event topology is very favorable and a measurement indeed seems possible. Many of the detector groups at SLC and LEP have studied the experimental problems and their conclusions are pretty uniform. We chose here the study discussed in the SLC workshop (reference 6 b), page 127.

The favorable topology arises from the fact that most of the energy in the process $Z^0 \rightarrow H^0\ell^+\ell^-$ goes to the virtual Z^0 and hence the two leptons which result from the decay of the virtual Z^0 have very high momenta. This can be seen from figure 26. The H^0 is produced with a fairly small fraction of the available energy and will decay mostly into two quark jets. In addition there is very little correlation between the H^0 direction and the e^+ or e^- direction and in most events the $e^\pm$ will be well separated from the H^0 decay products. The topology is schematically shown in figure 27.

The main source of background comes from the process $Z^0 \rightarrow t\bar{t}$ where both the t and $\bar{t}$ decay semi-leptonically. However requiring the angle between sphericity axis of the hadronic system (all particles except the ℓ^+ and ℓ^-) and the leptons to be $\gtrsim 200$ mrad virtually eliminates this background for $M_{H^0} \lesssim 40$ GeV/c^2. This cut loses very little signal ($\approx 6\%$) because there is no correlation between the direction of the leptons and the hadronic sphericity axis.

The mass of the hadronic system (the H^0) is obtained from the missing mass recoiling against the lepton pair. The experiment can be done with either a e^+e^- or $\mu^+\mu^-$ lepton pair providing that the energy resolution of the leptons is sufficiently good to see a peak in the missing mass. Figure 28 shows the results of a simulation in which $M_{H^0} = 10$ GeV/c^2 and the e^+e^- lepton final state was used. The electron energy is measured in a electromagnetic calorimeter with an energy resolution of $\sigma_E/E = 10\%/\sqrt{E}$. A very clear signal is seen with a mass resolution of ≈ 1 GeV/c^2. The background from $Z^0 \rightarrow$ hadrons is also shown in figure 28. To obtain equivalent H^0 mass resolution from the $\mu^+\mu^-$ final state requires $\sigma_p/p^2 \approx 0.1\%$. As noted before this search method will work for Higgs masses of $\lesssim 40$ GeV/c^2.

Assuming the search was successful and we found a peak in the recoil mass spectrum how do we know that we have discovered the Higgs scalar? We would have to verify that it decayed isotropically and that the couplings favored the heaviest fermion pair available.

We can measure the decay angular distribution as follows. First we would reconstruct the two jet directions from the particles associated with the jets. From the ℓ^+ and ℓ^- momenta we can reconstruct $\vec{P}_{H^0}$. Knowing M_{H^0} and $\vec{P}_{H^0}$, we can transform the jet directions into the H^0 center of mass and plot the decay angular distribution. (This method will work as long as we can make the assumption that the decay angular distribution is symmetric about $\theta^* = 90°$. This is because we don't know how to distinguish the jet from the anti jet (θ^* from $\pi - \theta^*$) and hence by plotting both we are assuming a symmetric decay distribution). Realistically the major problem with this procedure will be the limited statistics. Optimistically one might have ≈ 50 events to play with.

Now how about measuring if the coupling is proportional to m_f^2? Here the procedure would depend on M_{H^0}. Suppose, as is likely, that $M_{H^0} > 10$ GeV/c^2

in which case $H^0 \to b\bar{b}$ almost exclusively (see figure 23). We will see in the next section that using a vertex detector one can expect to tag events containing two b jets with an efficiency $\gtrsim 50\%$ and this with very little contamination from c jets. This can be done because the b quark has a long measured ($\sim$ psec) lifetime. So one would subject the $H^0\ell^+\ell^-$ candidate events to this test and if indeed half (= tag efficiency) the events were tagged as having a b jet, one would feel fairly confident that the H^0 decayed predominantly to $b\bar{b}$. If $M_{H^0} < 10$ GeV/c^2 the obvious signal to look for would be $H^0 \to \tau^+\tau^-$.

To summarize the H^0 search then it is probable that if $M_{H^0} \lesssim 40$ GeV/c^2 it can be found at the Z^0 . We will require a machine with excellent luminosity – $\langle\mathcal{L}\rangle > 10^{30}\ cm^{-2}\ sec^{-1}$ – and a detector with good electromagnetic calorimetry and/or momentum resolution. All the LEP and SLC detectors appear capable of doing this measurement. With sufficient statistics ($\gtrsim 50$ events) the H^0 decay angular distribution and coupling can probably be inferred.

5.6 What Will We Learn From $Z^0 \to$ Hadrons?

An obvious question is can we learn anything form $Z^0 \to$ hadrons which cannot be obtained from PETRA ($E_{c.m.} \lesssim 46$ GeV) and PEP ($E_{c.m.} \lesssim 36$ GeV)? The answer is yes and probably the main reason is that the Z^0 offers a very large statistical advantage over the PEP and PETRA machines. At present the largest PEP/PETRA hadronic dataset is the MARK II which has 100,000 hadronic events at a PEP energy of $E_{c.m.} = 29$ GeV. It has taken three years to accumulate this data and the present performance of PEP is that a good PEP year is worth 60,000 hadronic events. Contrast this with the expectation that a good SLC/LEP year will yield $\approx 180 \times 10^4$ hadronic events or 30 times as much as PEP. So there will be a considerable improvement in statistics. We now examine some of the physics which will be covered.

QCD Tests

As discussed by the authors in reference 17 (and probably many others) the QCD corrections to the Z^0 hadronic final states are exactly those calculated for lower energy e^+e^- interactions. In particular one recovers the familiar Sterman–Weinberg formula. All the usual low energy tools like sphericity, thrust, etc. are equally useful at the Z^0 . The familiar 3 jet Dalitz plot distributions for $e^+e^- \to Z^0 \to qqg$ are the same as for the continuum:

$$\frac{d^2\Gamma(Z^0 \to 3\text{ jets})}{dx_1 dx_2} = \Gamma(Z^0 \to \text{hadrons})\ \frac{2\alpha_s(M_Z)}{3\pi}\ \frac{(x_1^2 + x_2^2)}{(1-x_1)(1-x_2)}$$

where x_i ($i = 1,2,3$) are the fractional parton energies ($x_i = 2E_i/E_{c.m.}$) and $\sum_i x_i = 2$. We can study the three jet events at the Z^0 in much the same way as we study them at PETRA and PEP. These studies will probably be easier at

the Z^0 because the jet cone angles will be $\sim 2-3$ times smaller ($\approx 1/E_{\rm jet}$) than at PEP or PETRA. Hence the problems of which particles belong to which jet should be easier. This will provide more reliable measurements of x_i, quark and gluon jet multiplicities and jet directions. In addition the efficiency for finding well reconstructed 3 jet events should be higher than at lower energies. And of course there will be a copious supply of 3 jet events. Simulations have shown that about 60% of the produced three jet events are cleanly reconstructed which would yield about 5×10^4 reconstructed 3 jet events/10^6 produced Z^0's. By contrast the MARK II has about 5×10^3 reconstructed 3 jet events and many of the PETRA results at 34 GeV have been published on $\lesssim$ 1000 3 jet events. Back to what we will learn.

We will try to measure α_s, a task which has been frustrating at lower e^+e^- energies.[18] Part of the problem with the lower energy measurements has been understanding the QCD corrections and removing the model dependence. Combining the new data at $E_{c.m.} = M_{Z^0}$ with the low energy data will allow one to measure some of these effects which are now parametrized in a variety of models. α_s would be measured using the same techniques as at lower energies (see reference 18 as an example) namely studying the Dalitz plot distributions, or measuring the ratio of 3 jet to 2 jet events, or measuring particle energy correlations, event shapes, etc. I expect the model dependent problems encountered at lower energies will be much improved at the Z^0 . However new model dependent effects may prove troublesome, an example of which is the appearance, at higher energies, of many soft gluons. I would not speculate with confidence that α_s will be more easily measured at the Z^0 , but in all probability things will be better.

With many reconstructed jets at energies hitherto not available in e^+e^-, more information will be gained on the quark fragmentation process. In particular the question of whether quarks and gluons fragment differently can be studied. It has been argued in many places (see reference 19 for but a few) that for highly perturbative parton regimes (high energy partons) gluon jets should be considerably broader than quark jets. This is an important test because it arises from the gluon self–coupling which relates directly to the non–abelian nature of QCD. The difference in the fragmentation of quarks and gluons comes about from the fact (see figure 29) that the color charge at the triple gluon vertex is 9/4ths larger than at the quark–quark–gluon vertex. The ratio of the cone angle δ(a la Sterman and Weinberg) of a gluon and a quark jet is given roughly by

$$\delta_g(E) \approx \delta_q(E)^{4/9}$$

where δ is measured in radians. The cone angle δ is such that most ($\gtrsim$ 90%) of the parton energy is contained in the cone. At the Z^0 one expects $\delta_q \simeq 10°$ which would imply a gluon jet of the same energy would have $\delta_g \approx 27°$. Such

large differences should be seen easily and the Z^0 3 jet events should provide a meaningful test of differences in quark and gluon jets.

Flavor Tagging

We have already seen earlier in this section that $t\bar{t}$ events can easily be tagged using event shape parameters or high P_t leptons. The advantage of the high P_t tag is that the sign of the lepton charge flags which jet is t and which is the $\bar{t}$. The importance of this will become apparent soon. Studies by the MARK II upgrade group have shown that the high P_t lepton tag has high efficiency for selecting $t\bar{t}$ events and in addition backgrounds (from $b\bar{b}$ mainly) are small. Requiring a high P_t lepton they find $\approx 1.4 \times 10^4$ tagged $t\bar{t}/10^6$ Z^0's with a background of $< 10\%$. This number will be diluted if $M_t > 25$ GeV/c^2 according to the curve in figure 11.

How about tagging $b\bar{b}$ events? The B meson appears[20] to have a lifetime on the order of 1 psec. At the Z^0 , they will travel $\gamma\beta c\tau \approx 3$ mm on average before they decay. The decay particles of the B meson, when extrapolated back towards the primary vertex, will appear to "miss" the primary vertex (see figure 30). The amount by which they "miss" is called the impact parameter, b. Large impact parameter tracks will signal the decay of a long lived particle. From simulations one finds that for $\tau_B = 10^{-12}$ secs typical tracks from B meson decay in $Z^0 \rightarrow b\bar{b}$ events have $b \gtrsim 200\ \mu$. This can be contrasted with expected measurement errors of $50 - 100\ \mu$. In a study done by the MARK II Upgrade Group,[21] efficiencies of $\geq 50\%$ were found for tagging events of the type $Z^0 \rightarrow b\bar{b}$. The technique used was to require at least 3 tracks in a jet with $\geq 3\sigma_b$ where σ_b was the error in the measurement of the track's impact parameter. Multiple scattering in the apparatus walls can cause tracks to have large impact parameters and hence provide bogus tagging information. Requiring three tracks with a substantial impact parameter alleviates this problem. In addition the invariant mass of the three large impact parameter tracks was required to be > 1.95 GeV/c^2 which eliminates almost all background from D decays. The tagged $b\bar{b}$ events sample was found to have $< 10\%$ background from non $b\bar{b}$ events.

Using this efficiency as prototypical, one would expect 6.8×10^4 tagged $b\bar{b}$ events/10^6 Z^0 events. If in addition one required an electron or a muon to distinguish quark and antiquark b jets, one would have a tagging efficiency of about 8×10^3 $b\bar{b}/10^6$ Z^0 events.

So it seems as if one will be able to tag b and t jets at the SLC and LEP with impressive event yields. What physics can be done? Clearly the fragmentation process, both longitudinal and transverse, for heavy quarks can be studied. Jet multiplicity can be studied. Comparisons with low energy data will provide additional information on the fragmentation process.

The B lifetime will be measured with better precision and better statistics than at PEP. Current τ_B measurements rely on $\lesssim 300$ events which affects not

only the statistical error in τ_B but also limits the ability of the experiments to understand their systematics. Presently the systematics are limiting the measurements at the $\sim 25\%$ level. We can use the tagged $b\bar{b}$ events to measure the B meson lifetime and divide the events into two jets. The one jet will provide the b jet tag as discussed above. The other jet can be used in an unbiased way to measure the B lifetime. Estimates from simulations done by the MARK II upgrade group indicate that using the same method employed at PEP[20] a systematic error of $\sim 5\%$ should be achieved for τ_B.

With tagged $b\bar{b}$ and $t\bar{t}$ events we could measure the charged $2/3rds$ and $-1/3rd$ quark couplings. Recall (section 3) that if we measure

$$R_q = \frac{\sigma_{q\bar{q}}}{\sigma_{\text{point}}} \propto (a_q^2 + v_q^2)$$

and

$$A_{F-B}^q = \frac{3a_e v_e a_q v_q}{(a_q^2 + v_q^2)(a_e^2 + v_e^2)}$$

we can obtain a_q and v_q. (We are assuming a_e, v_e are measured as discussed earlier in this section.) With a tagged sample of $b\bar{b}$ and $t\bar{t}$ we can make these measurements. For the forward-backward asymmetry we need to distinguish q from $\bar{q}$, so we will have to use events with an electron or muon. Even with this restriction the statistical errors in the measurement of the couplings will be $\lesssim 2\%$ for 10^6 Z^0 events. The R_q measurement requires an accurate measurement of luminosity which will be possible at the $\leq 5\%$ level. In order to determine the quark direction one will use the thrust axis. At the Z^0 this will be well determined and should not effect the quality of the measurement of A_{F-B}^q. It will be very important to have good detector coverage at small θ angles. The solid angle (25% of 4π) for which $\theta < 40°$ contains as much asymmetry information as the remaining 75% of 4π. Based on those considerations, I would expect one could measure the b and t couplings to $\lesssim 10\%$. This would be an important test of the Standard Model.

We return now to the question posed earlier. Suppose we discover a new heavy quark at the SLC or LEP. How do we know its charge? Is it the t or a b'? The key is the difference in the couplings. Simple substitution using the values in Table I gives

$$A_{F-B}^t = 6.5\%$$

and

$$A_{F-B}^b = 13\% \quad .$$

From the statistics of the tagged samples alone $\delta A \simeq 1\%$ for 10^6 Z^0 events. If systematic problems are not too large, A_{F-B} should distinguish between charged 2/3 and -1/3 quarks.

6. GOING BEYOND THE STANDARD MODEL

Possibly the most fun at the Z^0 machines will be the surprises. I will look back at these lectures and realize that the exciting Z^0 physics wasn't in them! I certainly hope so!! Well how about some "predictable" surprises – namely things which spoil the tidy Standard Model predictions.

6.1 NON-MINIMAL HIGGS SCHEME; SEARCHING FOR CHARGED HIGGS

We have assumed a minimal Higgs structure until now – how about a Higgs structure with two complex doublets. (8 fields):

$$\phi_1 = \begin{pmatrix} \phi_1^+ \\ \phi_1^0 \end{pmatrix} \qquad \langle\phi\rangle_0 = v_1$$

$$\phi_2 = \begin{pmatrix} \phi_2^+ \\ \phi_2^0 \end{pmatrix} \qquad \langle\phi\rangle_0 = v_2$$

and $v_1 + v_2 = v = \sqrt{2}G_F$. After symmetry breaking, 3 of the fields are consumed in generating $W^\pm$, Z^0 masses and five physical particles remain. They are:

Two neutral scalars	H_1^0, H_2^0
One pseudoscalar	h^0 (the axion in some models)
and two charged pseudoscalars	H^+, H^- .

Fermion mass generation is achieved by arranging for ϕ_1 to give mass to the charged 2/3 quarks and ϕ_2 to give mass to the charge -1/3 quarks. This arrangement avoids any flavor changing neutral currents. What about the Higgs couplings? The usual scalar rule applies – the coupling is strongest to the heaviest fermions:

$$g_{fH_1} = \frac{1}{v_1} M_{u,c,t} \qquad g_{fH_2} = \frac{1}{v_2} M_{d,s,b} \; .$$

However, there is a problem because the theory doesn't tell us v_1/v_2. Since $M_c > M_s$ and $M_t > M_b$ maybe $v_1 > v_2$ but certainly this is not guaranteed. Another complication for experimental tests is that by analogy with the $W^\pm$ sector we could have mixing in the $H^\pm$ sector. We will have an analog of the Kobayashi–Maskawa matrix and we have no knowledge of the elements of this matrix. How would we search for such charged scalars? The only possible way at

the Z^0 is via $e^+e^- \to Z^0 \to H^+H^-$. How much would such a process contribute to the Z^0 width? From our previous discussion we can write

$$\Gamma(Z^0 \to H^+H^-) = \frac{G_F M_Z^3}{24\pi\sqrt{2}}(v_H^2 + a_H^2) \quad .$$

Now at the Z^0 H^+H^- vertex only the vector coupling occurs. The axial coupling is absent because the parity of two identical spin 0 particles in an $L = 1$ state is -1. For the $H^\pm$, $T_3 = \pm 1/2$ and hence $v_H = 1/2(1 - 4\sin^2\theta_W)$. So we find

$$\frac{\Gamma(Z^0 \to H^+H^-)}{\Gamma(Z^0 \to \mu^+\mu^-)} = \frac{v_H^2}{(v_\mu^2 + a_\mu^2)} \frac{1}{4} \beta_{H^\pm}^3 = 3.6 \times 10^{-3} \beta_{H^\pm}^3$$

where $\beta_{H^\pm}$ is the velocity of the $H^\pm$. Hence $B(Z^0 \to H^+H^-) \leq 10^{-4}$ - far too small to detect in the presence of the $Z^0 \to$ hadron events. So in fact there is no good way to search for $H^\pm$ at the Z^0 .

A note in passing about technicolor which I will not discuss further. The $H^\pm$ which we have been discussing could equally well be the $P^\pm$ technipion. Now $T_3 = \pm 1$ for the technipion and hence $B(Z^0 \to P^+P^-) \simeq 10^{-2}\beta_{P^\pm}^3$. This would still be hard to look for, but worth a try. The main source of background will be four jet events from QCD which occur at a rate of $\alpha_S^2 \simeq 2\%$.

6.2 The Generation Puzzle - Searching for New Generations

The discovery of the τ and the b quark has led to a very beautiful symmetry between the quark and lepton sectors. Nature at present appears to have three generations of both quarks and leptons. While this symmetry is indeed attractive, we are led to an obvious question - why three generations? Why not five or ten? We readily understand the need for one generation - our very being is dependent on it. But more than one generation seems superfluous and it is interesting to speculate on why nature chose to replicate itself in this strange way.

The distinguishing generation element is mass - successive generations have higher masses. A perfectly defensible reason why we see three generations then is that the energy of our machines is not sufficient to yield the next generation(s). The prospect of higher energy machines implies more quarks and leptons. We may go to our theoretical friends and ask them where we need to look; where will the next generation appear? The answer is that none of the current theories understands the generation puzzle and no mass predictions exist.

The prospect of a factor of $\gtrsim 2$ in available energy, plus the large rate makes the Z^0 a good place to look for new generations. How do we search for new generations? There are three obvious possibilities

a) Search for a new charged lepton, $L^{\pm}$,

b) Search for a new $Q = -1/3$ quark, and

c) Search for more ν's.

We do not include searches for $Q = 2/3$ quarks because if such a quark were found, it would satisfy our need for the top quark. Consider the search for $L^{\pm}$. The $W^{\pm}$ which mediate the decays of $L^{\pm}$ is democratic with respect to fermion coupling strengths. Allowing for three quark colors we have

$$B(L^{\pm} \to \ell^{\pm}\nu\nu) = \frac{1}{12} = 8\%$$

and

$$B(L^{\pm} \to \text{hadrons}) = 76\% \ .$$

(These numbers will be modified slightly by QCD corrections but, for the argument being made here, these small modifications are unimportant.) We will therefore be able to use the standard low multiplicity searches for $L^{\pm}$ which will be pair produced with $B(Z^0 \to L^+L^-) = 3\%\ \beta_{L^{\pm}}(3 - \beta^2_{L^{\pm}})/2$ where β_L is the heavy lepton velocity. It would be like searching for the τ all over again. From PETRA we know that $M_{L^{\pm}} > 18$ GeV/c^2 and hence $\beta_{L^{\pm}} \leq 0.92$. As an example one might search for $e^{\mp}\mu^{\pm}$ events. For $M_{L^{\pm}} = 40$ GeV/c^2 ($\beta_L = .4$), there would be 100 $e^{\pm}\mu^{\mp}$ events / 10^6 Z^0 events. In the channel ex or μx there would be 10^3 events / 10^6 Z^0 events. So it is easy to search for $L^{\pm}$ at the Z^0 as long as $M_{L^{\pm}} < M_{Z^0}/2$.

We have already discussed how to find a new heavy quark and how the charge asymmetry A_{F-B} can be used to separate charge -1/3 and charge 2/3 quarks. If a new heavy quark were found with a charge -1/3 this would signal the presence of a new generation.

Finally we discuss the search for additional ν's. We derived in section 3 $\Gamma(Z^0 \to \nu\bar{\nu}) \simeq 170$ MeV and decided in section 4 that we could possibly measure Γ_{Z^0} with a precision $\lesssim 100$ MeV. But how do we know that the additional width comes from a 4th ν? Is there a way to count the number of ν species?

The answer is possibly, but not by running on the Z^0 , but rather by running above the Z^0 and observing the radiative transition

$$e^+e^- \to \gamma Z^0$$
$$\hookrightarrow \nu\bar{\nu} \ .$$

One can chose an $E_{c.m.}$ such that the mass recoiling against the photon is M_{Z^0}. In this way one gets an enhanced event rate. This measurement is discussed by Barbiellini et al.[22] and the theoretical background can be found in reference 23.

The Feynman diagrams are shown in figure 31. It turns out that the $W^{\pm}$ exchange diagrams are very small (see figure 32) and can be ignored. If this is done then

$$\frac{d^2\sigma}{dxdy} \simeq \frac{G_F \alpha S f(x,y)(v_\nu^2 + a_\nu^2) N_\nu}{\{[1 - S(1-x)/M_Z^2]^2 + \Gamma_Z^2/M_Z^2\}}$$

where

$$f(x,y) = \frac{(1-x)[(1-x/2)^2 + x^2y^2/4]}{6\pi^2 x(1-y^2)}$$

and

$$x = 2E_\gamma/E_{c.m.} \quad , \quad y = \cos\theta_\gamma$$

$$N_\nu = \#\text{ of } \nu \text{ species} .$$

A measurement of $\sigma_{\nu\bar{\nu}} = \int \frac{d^2\sigma}{dxdy}\, dxdy$ measures directly the number of neutrino species in the world! Each new species adds about 33% to $\sigma_{\nu\bar{\nu}}$. We need to chose $E_{c.m.}$ sufficiently high so that the backgrounds from $e^+e^- \to e^+e^-\gamma$ are sufficiently small. Choosing[22] $E_{c.m.} = 105$ GeV and integrating over $y = \cos\theta_\gamma$ in the interval $20° < \theta_\gamma < 160°$ yields the differential cross-section shown in figure 32. We can now integrate over the Z^0 reflection peak, namely require experimentally that one sees a photon of energy 14 ± 2.5 GeV. The cross section so obtained is $\sigma_{\nu\bar{\nu}} = 0.025$ nb for $N_\nu = 3$. Each new generation will contribute $\sigma_{\nu\bar{\nu}} \simeq 0.008$ nb. For $\langle\mathcal{L}\rangle = 3\times10^{30}\ cm^{-2}\ sec^{-1}$ the event rate is $2/\text{day}/\nu$ species. A 50 day run would yield 100 events/ν species – easily enough to measure N_ν.

The experimental signal is very simple – one hard ($E_\gamma = (14 \pm 2.5)$ GeV) photon in the angular range $20° < \theta < 160°$ and nothing else. What about backgrounds from QED processes like $e^+e^- \to e^+e^-\gamma$ and $e^+e^- \to 3\gamma$? The former background is potentially much larger. Suppose we observe a 14 GeV photon from the $e^+e^-\gamma$ process at $\theta = 20°$. The P_t of this photon will be balanced by the $e^{\pm}$ which radiated it. To a reasonable approximation we can write

$$\tan\theta_{e^\pm} \simeq \theta_{e^\pm} = \frac{E_\gamma \sin 20°}{E_{e^\pm}} \simeq 6° \quad .$$

In other words there is a minimum angle, θ_{min}, beyond which one must see an electron (or positron) if one sees the 14 GeV photon with $20° < \theta < 160°$. The real kinematics and cross section appear in figure 33. With a veto for the $e^{\pm}$ down to $\theta = 6°$, the signal to noise will be 40:1.

The detector required for this experiment is very simple. Electromagnetic shower counters down to within 6° of the beamline and a charged particle tracker (no magnet needed) for $20° < \theta < 160°$ to ensure that the γ is not an electron. All the SLC and LEP detectors are equipped to do this experiment.

Like all cute ideas, this experiment does have a problem. It does not necessarily measure N_ν but rather the number of neutral, stable, weakly coupled species in the world. An example of a process which would contribute to the counting rate of this experiment is $Z^0 \to \tilde{\nu}\,\tilde{\bar{\nu}}$, where $\tilde{\nu}$ is a sneutrino. We will comment on this later.

6.3 SUPERSYMMETRY

A very large part of this Summer School was devoted to Supersymmetry and there is no point in my giving an outline here. Reference 24 by Kane and Haber is an excellent "All You Ever Wanted to Know About SUSY" reference and I borrowed liberally from it for these lectures. There are many models and many decay schemes and what I write down here is presumably true in some model(s). But this doesn't mean that it is correct – i.e. SUSY doesn't demand it, rather the model does.

Production cross sections for the partners of the normal fermions are characteristic of scalars namely

$$R_{\tilde{s}\,\tilde{\bar{s}}} = \frac{1}{4} R_{f\bar{f}} \quad .$$

Here $\tilde{s}$ indicates a SUSY scalar whose normal partner is denoted by f. However there are two SUSY partners for each normal fermion so in reality

$$R_{\tilde{s}\,\tilde{\bar{s}}} = \frac{1}{2} R_{f\bar{f}}$$

and

$$\frac{d\sigma_{\tilde{s}\,\tilde{\bar{s}}}}{d\cos\theta} = \frac{1}{2}\beta^3 \sin^2\theta\, \sigma_{f\bar{f}} \quad .$$

So SUSY scalars could add as much as $\sim 50\%$ to the width of the Z^0. As we said previously, if Γ_Z is too wide there could be many reasons for it. One would have to search for each possibility separately.

Scalar leptons will be copiously produced and $B(Z^0 \to \tilde{\ell}^+\tilde{\ell}^-) = 1\frac{1}{2}\%\ \beta^3$ where β is the scalar lepton velocity. Presumably $\tilde{\ell}^\pm \to \ell^\pm\ \tilde{\gamma}$ and, assuming the $\tilde{\gamma}$ is stable, one gets a very distinctive signature namely events at the Z^0 which have two high energy leptons (e^+e^-, $\mu^+\mu^-$ or $\tau^+\tau^-$) with large missing P_t and energy. The presence of a stable light particle ($\tilde{\gamma}$) in the decay chains of all the SUSY particles implies that SUSY events are characterized by missing P_t and energy. This is a key element in the search for SUSY signatures.

For scalar quarks $B(Z^0 \to \tilde{u}\,\tilde{\bar{u}}) = 6.6\%\ \beta^3$, $B(Z^0 \to \tilde{d}\,\tilde{\bar{d}}) = 5.3\%\ \beta^3$ where β is the quark velocity. The scalar quark will decay to a quark and a gluino or $\tilde{\gamma}$ and hence one has events with two jets which are not back to back but have

substantial missing P_t and energy. Again this is a distinctive signature and, provided β is not too small, there is copious production.

For scalar neutrinos $B(Z^0 \to \tilde{\nu}\,\tilde{\bar{\nu}}) = 3\%\ \beta^3$ where β is the $\tilde{\nu}$ velocity. In order to discuss this channel further requires a decay scheme for the $\tilde{\nu}$. The schemes are complicated by the fact that one has no idea of the scalar electron, scalar ν, . . . masses. Certainly a prominent decay mode will be $\tilde{\nu} \to \nu\tilde{\gamma}$ which is an invisible mode which could have a branching fraction $\simeq 0.6$. There are also multiple charged particle modes possible as known in figure 34 taken from Barnett et al.[25] How much will $Z^0 \to \tilde{\nu}\,\tilde{\bar{\nu}}$ contribute to the ν counting experiment? The contribution per SUSY species relative to a ν species will be

$$N_{\tilde{\nu}}/N_\nu = B^2(\tilde{\nu} \to \nu\tilde{\gamma})\ \frac{\Gamma(Z^0 \to \tilde{\nu}\,\tilde{\bar{\nu}})}{\Gamma(Z^0 \to \nu\bar{\nu})} \approx 0.2$$

where I have used $B(\tilde{\nu} \to \nu\tilde{\gamma}) \simeq 0.4$. In all likelihood then, it will be hard to see a scalar ν species in the neutrino counting experiment.

The multicharge decays shown in figure 34 could generate some spectacular events at Z^0. The topology

$$Z^0 \to \tilde{\nu}\,\tilde{\bar{\nu}} \begin{cases} \to \nu_e e^- e^+ \tilde{\gamma} \\ \to \nu\tilde{\gamma} \end{cases}$$

would yield an electron and positron in one hemisphere of the detector and nothing else! Even if $B(\tilde{\nu} \to \nu_e e^+ e^- \tilde{\gamma}) \approx 10^{-3}$, 10^6 Z^0's would yield ~ 40 such events! Another interesting topology would be

$$Z^0 \to \tilde{\nu}\,\tilde{\bar{\nu}} \begin{cases} \to e^- q\bar{q}\tilde{g} \\ \to \tilde{\gamma}\nu \end{cases}$$

yielding an electron, two quark jets and a gluino in one hemisphere and nothing visible recoiling against them. The electron energy is expected to be large ($\langle P_e \rangle \approx 8$ GeV) making them easy to detect. Certainly if SUSY is correct there is a chance that we could see some spectacular events at the Z^0 .

What about the charginos $\omega^\pm$, $h^\pm$ which are the spin 1/2 partners of the $W^\pm$ and $H^\pm$. Since they couple weakly, these particles look like heavy leptons $L^\pm$ discussed earlier. They decay via

$$h^\pm\ ,\ w^\pm \to W^\pm\tilde{\gamma} \quad \hookrightarrow \ell^\pm\nu \text{ or } q\bar{q}\ .$$

The decay will be the same as $L^\pm \to W^\pm\nu$ except for effects arising from large $\tilde{\gamma}$ mass. How are they distinguished from $L^\pm$? Consider for the moment the

unmixed case for which the weak couplings are

$$v = (T_{3L} + T_{3R} - 2Q \sin^2 \theta_W)$$

$$a = T_{3L} - T_{3R}$$

with

$$T_{3L} = T_{3R} = \pm 1 \qquad \text{for } w^{\pm}$$

$$T_{3L} = T_{3R} = \pm 1/2 \quad \text{for } h^{\pm} .$$

Hence $v_{W^{\pm}} = 1.56$, $v_{h^{\pm}} = 0.56$ and $a_{w^{\pm}} = a_{h^{\pm}} = 0$. So for this unmixed case

$$\frac{\Gamma(Z^0 \to w^+ w^-)}{\Gamma(Z^0 \to \tau^+ \tau^-)} = 9.6$$

and

$$\frac{\Gamma(Z^0 \to h^+ h^-)}{\Gamma(Z^0 \to \tau^+ \tau^-)} = 1.2 .$$

Hence charginos could add as much as $\sim 33\%$ to Γ_Z. The search for $w^{\pm}, h^{\pm}$ proceeds exactly as the search for $L^{\pm}$ discussed earlier.

How does one distinguish the $L^{\pm}$ from the $w^{\pm}$, $h^{\pm}$? Their weak interactions are very different! The charge asymmetry is

$$A_{F-B} = \frac{3 v_e a_e v_f a_f}{(v_e^2 + a_e^2)(v_f^2 + a_f^2)}$$

$$= 4.3\% \text{ for } L^{\pm}$$

$$= 0 \text{ for } w^{\pm}, h^{\pm} \text{ in unmixed cases.}$$

We have considered the simplest unmixed case. Suppose the $w^{\pm}$ and $h^{\pm}$ are maximally mixed in states $\tilde{w}_1$ and $\tilde{w}_2$. Then

$$\frac{\Gamma(Z^0 \to \tilde{w}_1^+ \tilde{w}_1^-)}{\Gamma(Z^0 \to \tau^+ \tau^-)} = \frac{\Gamma(Z^0 \to \tilde{w}_2^+ \tilde{w}_2^-)}{\Gamma(Z^0 \to \tau^+ \tau^-)} = 5.5$$

and

$$A_{F-B}^{\tilde{w}_1} = 14\%$$

$$A_{F-B}^{\tilde{w}_2} = -14\% .$$

Of course we have no guidance from the theory as to what level of mixing, if any, there is.

7. ACKNOWLEDGEMENTS

I spent a very enjoyable week at Ann Arbor and found it exciting and rewarding to be with so many enthusiastic students and co–lecturers. I thank them for their interest and enrichment. I wish to thank the members of the University of Michigan physics department for their wonderful hospitality and in particular I wish to thank Marty Einhorn and Gordy Kane. My thanks also to the SLAC publications office for preparing this writeup in a timely fashion despite receiving it so close to the deadline.

8. REFERENCES

1. R. Hollobeek, NIM 184, 333 (1981).
2. ECFA 81/54, General Meeting on LEP, Villars–sur–Ollon, Switzerland, June 1981.
3. SLAC Linear Collider Conceptual Design Report, SLAC–299 (June 1980); B. Richter, SLAC-PUB-2854 (1981).
4. S. Ozaki, Proceedings of the 1981 International Symposium on Lepton and Photon Interactions at High Energies, Bonn, 1981, p. 935.
5. C. Y. Prescott, SLAC-PUB-2854 (1981); Proceedings of the SLC Workshop, SLAC–247 (March 1982).
6. (a) CERN Yellow Reports 76-18 (1976) and 79-01 (1979). (b) Proceedings of the SLC Workshop on Experimental use of the SLC; SLAC–Report–247 (1982). (c) Proceedings of the Cornell Z^0 Theory Workshop; CLNS 81-485.
7. LEP detectors:
   OPAL CERN/LPC/83-4
   L3 CERN–Proposal–LEP–L3
   ALEPH CERN/LPC/83-2
   DELPHI DELPHI–83–66/1
   SLC detectors:
   MARK II CALT–68–1015
   SLD SLD Design Report; Preliminary Edition only.
8. C. Quigg – Gauge Theories of the Strong, Weak and Electromagnetic Interactions.
9. J. D. Jackson and D. Schame, NIM 128, 13 (1975).
10. Y–S. Tsai, Phys. Rev. D4, 2821 (1971).
11. W. Marciano and A. Sirlin, Proceedings of the Cornell Z^0 Theory Workshop, page 20; M. Veltman, Phys. Lett. 91B, 95 (1980).

12. J. D. Bjorken and S. J. Brodsky, Phys. Rev. D1, 1416 (1970). For an explicit experimental application see TASSO Collaboration Phys. Lett. 86B, 243 (1979).

13. G. Tarnopolsky, SLAC-PUB-2842 (1981).

14. L. B. Okun, Proceedings of the 1981 International Symposium on Lepton and Photon Interactions at High Energies, Bonn, 1981, p. 1018.

15. J. D. Bjorken, SLAC–198 (1976).

16. J. Finjord, Physica Scripta, Vol. 21, 143 (1980).

17. W. Marciano et al., Phys. Rev. Lett. 43, 22 (1979); D. Albert et al., Nucl. Phys. B166, 460 (1980).

18. J. M. Dorfan, Proceedings of the 1983 International Symposium on Lepton and Photon Interactions at High Energies, Cornell University, p. 686.

19. M. B. Einhorn and B. G. Weeks, Nucl. Phys. B146, 445 (1978); K. Shizuya and S. -H. H. Tye, Phys. Rev. Lett. 41, 787 (1978).

20. MAC Collaboration, E. Fernandez, et al., Phys. Rev. Lett. 51, 1022 (1983); MARK II Collaboration, N. Lockyer et al., Phys. Rev. Lett. 51, 1316 (1983).

21. Ken Hayes, "*B* Tagging at the SLC," MARK II/SLC NOTE # 73.

22. G. Barbiellini, et al., Phys. Lett. 106B, 414 (1981).

23. E. Ma and J. Okada, Phys. Rev. Lett. 41, 287 (1978); K. Gaemers et al., Phys. Rev. D19, 1605 (1979).

24. G. Kane and H. Haber, UM-HE-TH83-17.

25. M. Barnett, et al., SLAC-PUB-3224.

Figure Captions

Figure 1 Side view of the collision of oppositely charged beams showing the "pinch" effect. The coordinate z is measured along the beam direction, x is transverse to the beam direction.

Figure 2 Schematic of the SLC machine.

Figure 3 The luminosity of the SLC as a function of $E_{c.m.}$.

Figure 4 The basic e^+e^- process where final states are produced via an intermediate photon or Z^0 . The notation is obvious except that q stands for a quark, H^0 the neutral Higgs scalar, $\ell^\pm$ a charged lepton, $H^\pm$ a charged Higgs scalar and $L^\pm$ a (new) heavy charged lepton.

Figure 5 Typical decays which result from the process in figure 4. The symbol g stands for a gluon.

Figure 6 Momentum distribution for different particle species produced in the decay of $Z^0 \rightarrow$ hadrons.

Figure 7 Distribution of the angle with respect to the jet axis for different particle species in $Z^0 \rightarrow$ hadron events.

Figure 8 A schematic of the Upgraded MARK II detector.

Figure 9 Feynman graphs used for calculations in the text.

Figure 10 The basic $e^+e^- \rightarrow \gamma,\ Z^0 \rightarrow f\bar{f}$ process.

Figure 11 The suppression factor of $t\bar{t}$ decays of the Z^0 as a function of M_t.

Figure 12 The charge asymmetry for $Z^0 \rightarrow \mu^+\mu^-$ as a function of $E_{c.m.}$.

Figure 13 Event topologies which could be used to study the decay $\tau^+ \rightarrow \pi^+\nu_\tau$ via the production process $Z^0 \rightarrow \tau^+\tau^-$. In (a) the τ^- decays to a single charged prong, whereas in (b) the τ^- is envisaged as decaying to three charged pions.

Figure 14 Momentum spectra for τ decay products for different values of $\sin^2\theta_W$ (a) for charged leptons arising from $\tau \rightarrow \ell\nu\bar{\nu}$ and (b) for pions arising from $\tau \rightarrow \pi\nu$.

Figure 15 The solid lines are taken from figure 14 with $\sin^2\theta_W = 0.23$. The data points result from a computer simulation which includes realistic detector components.

Figure 16 Weak radiative corrections which renormalize the value of $\sin^2\theta_W$ at the Z^0 .

Figure 17 First order final state radiative corrections (a) for photon emission and (b) for gluon emission.

Figure 18 The aplanarity distribution for events of the type $Z^0 \rightarrow q\bar{q}$. The distribution for $Z^0 \rightarrow t\bar{t}$ ($M_t = 30$ GeV/c^2) is shown separately from the lighter quarks.

Figure 19 The distribution of transverse momentum squared, with respect to the quark direction, for all muons in the event. Contributions from the different flavors are indicated in the figure.

Figure 20 Projection of the trajectories of charged particles, for an event of the type $Z^0 \rightarrow d\bar{d}$, on a plane perpendicular to the beams. The solonoidal field strength is 5 kG.

Figure 21 The same as for figure 20, except for $Z^0 \rightarrow t\bar{t}$ with $M_t = 30$ GeV/c^2.

Figure 22 The error in the determination of the top quark mass as a function of the top quark mass for a sample of $10^6 Z^0$ events. No systematic errors are included in this plot.

Figure 23 Decay modes of the neutral Higgs boson as a function of its mass.

Figure 24 The process $e^+e^- \rightarrow Z^0 \rightarrow H^0\ell^+\ell^-$.

Figure 25 The decay rate for $Z^0 \rightarrow H^0e^+e^-$ or $Z^0 \rightarrow H^0\mu^+\mu^-$ relative to $Z^0 \rightarrow \mu^+\mu^-$ which has a branching fraction of 3%.

Figure 26 Dilepton mass spectra for $Z^0 \rightarrow H^0 \ell^+ \ell^-$ for several choices of the Higgs mass. The normalization corresponds to 2000 hours of beam time at an average luminosity of $10^{30}\ cm^{-2}\ sec^{-2}$.

Figure 27 A schematic representation of the topology of the $Z^0 \rightarrow H^0 \ell^+ \ell^-$ events.

Figure 28 Scatter plot of $M(e^+e^-)$ versus recoil mass where a calorimeter with resolution $\sigma_E/E = 10\% /\sqrt{E}$ is assumed.

Figure 29 The contrasting "strengths" of the triple gluon vertex and the quark–quark–gluon vertex.

Figure 30 The production and subsequent decay of a B meson indicating the primary vertex, secondary vertex and the impact parameter (b) of one of the B decay tracks.

Figure 31 Lowest order Feynman diagrams contributing to the process $e^+e^- \rightarrow \gamma\nu\bar{\nu}$.

Figure 32 The differential cross section $d\sigma/dx$ ($x = 2E_\gamma/E_{c.m.}$) is shown as a function of E_γ for the process $e^+e^- \rightarrow \gamma\nu\bar{\nu}$. The calculation assumes $E_{c.m.} = 105$ GeV.

Figure 33 Estimates of the backgrounds from the processes $e^+e^- \rightarrow e^+e^-\gamma$ and $e^+e^- \rightarrow 3\gamma$ as a function of θ_{min} for $|y| \leq 0.94$ and $E_\gamma = 14.5 \pm 2.5$ GeV.

Figure 34 Possible decay modes for $\tilde{\nu} \rightarrow$ multiple charged particles taken from the model of Barnett et al., reference 25.

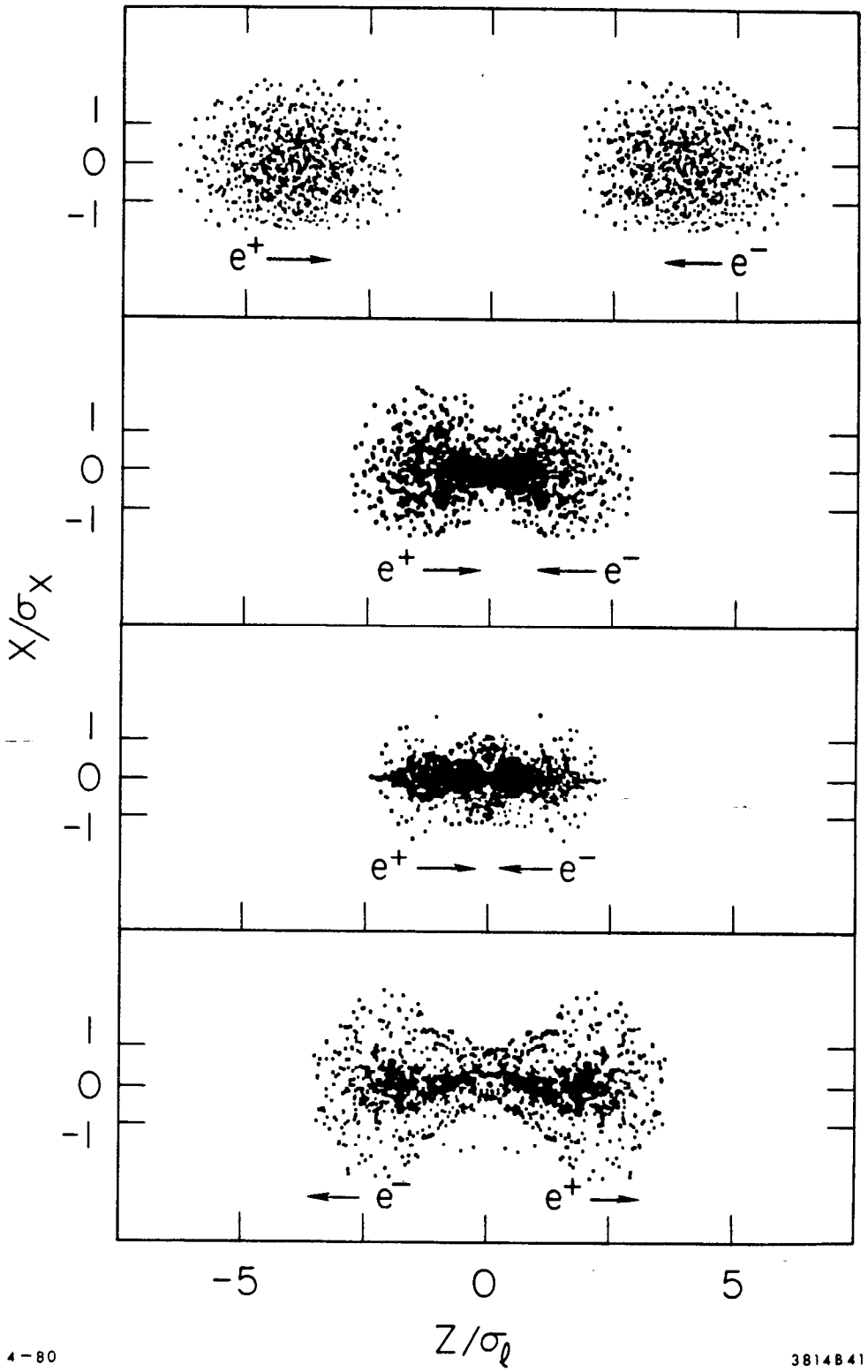

Fig. 1

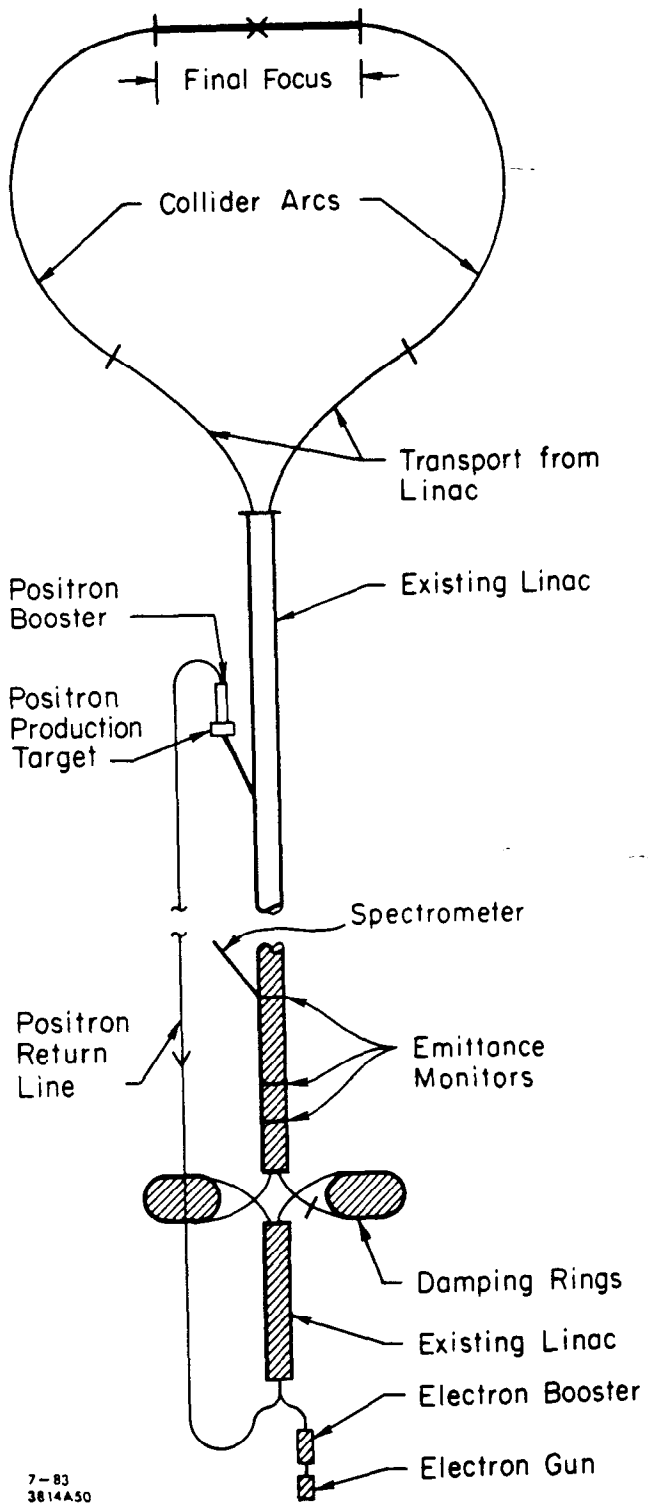
Final Focus
Collider Arcs
Transport from Linac
Existing Linac
Positron Booster
Positron Production Target
Spectrometer
Positron Return Line
Emittance Monitors
Damping Rings
Existing Linac
Electron Booster
Electron Gun
7-83
3814A50

Fig. 2

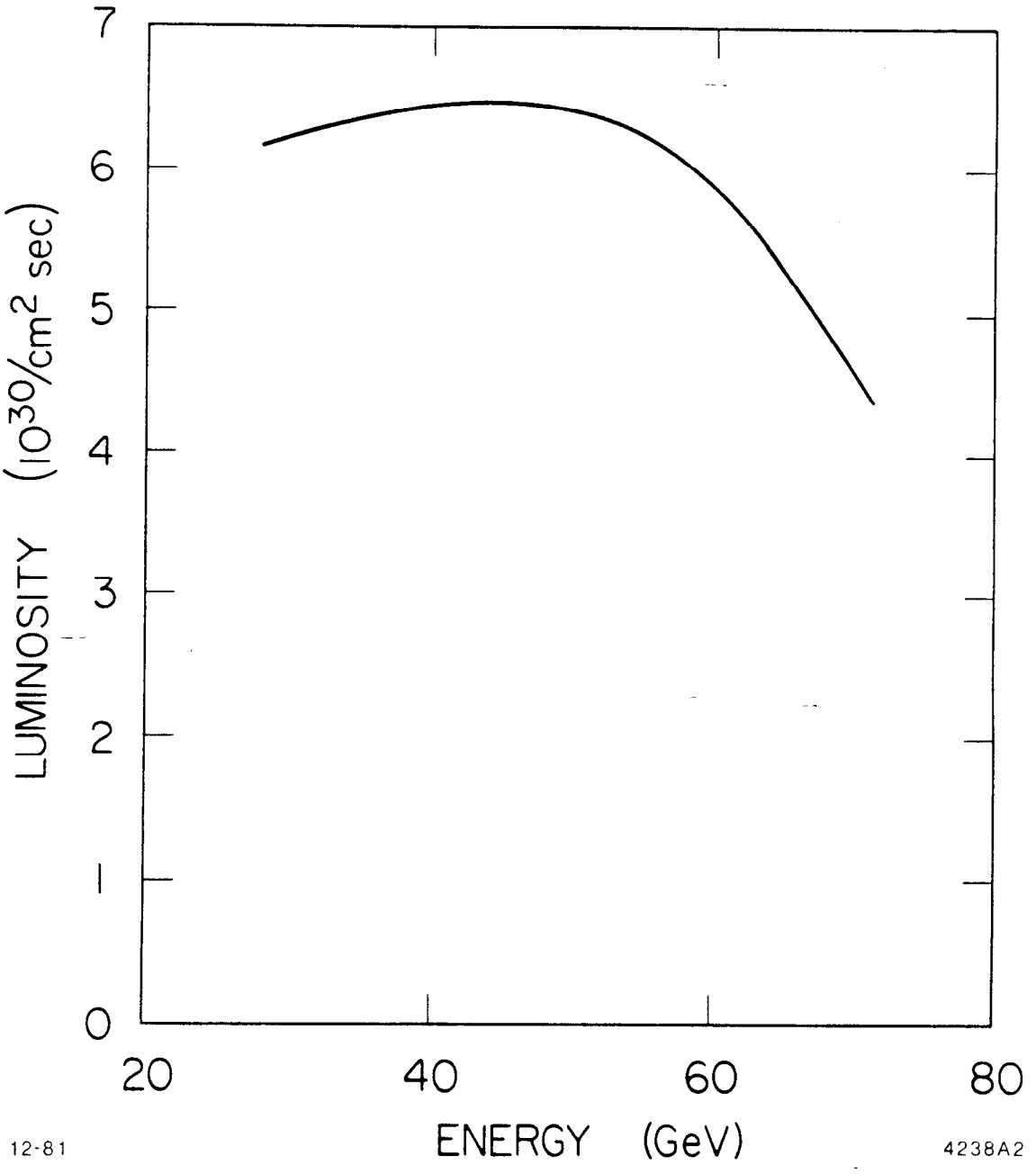
LUMINOSITY (10^30/cm^2 sec)
0
1
2
3
4
5
6
7
20
40
60
80
ENERGY (GeV)
12-81
4238A2

Fig. 3

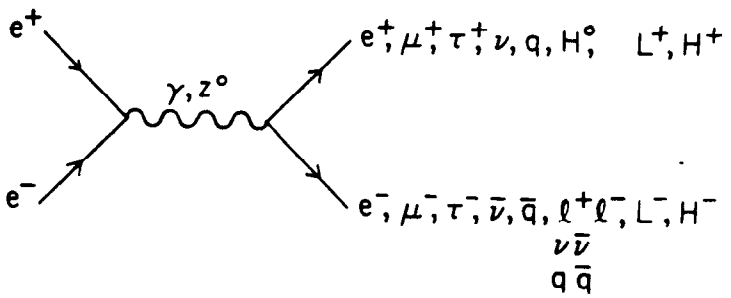

Fig. 4

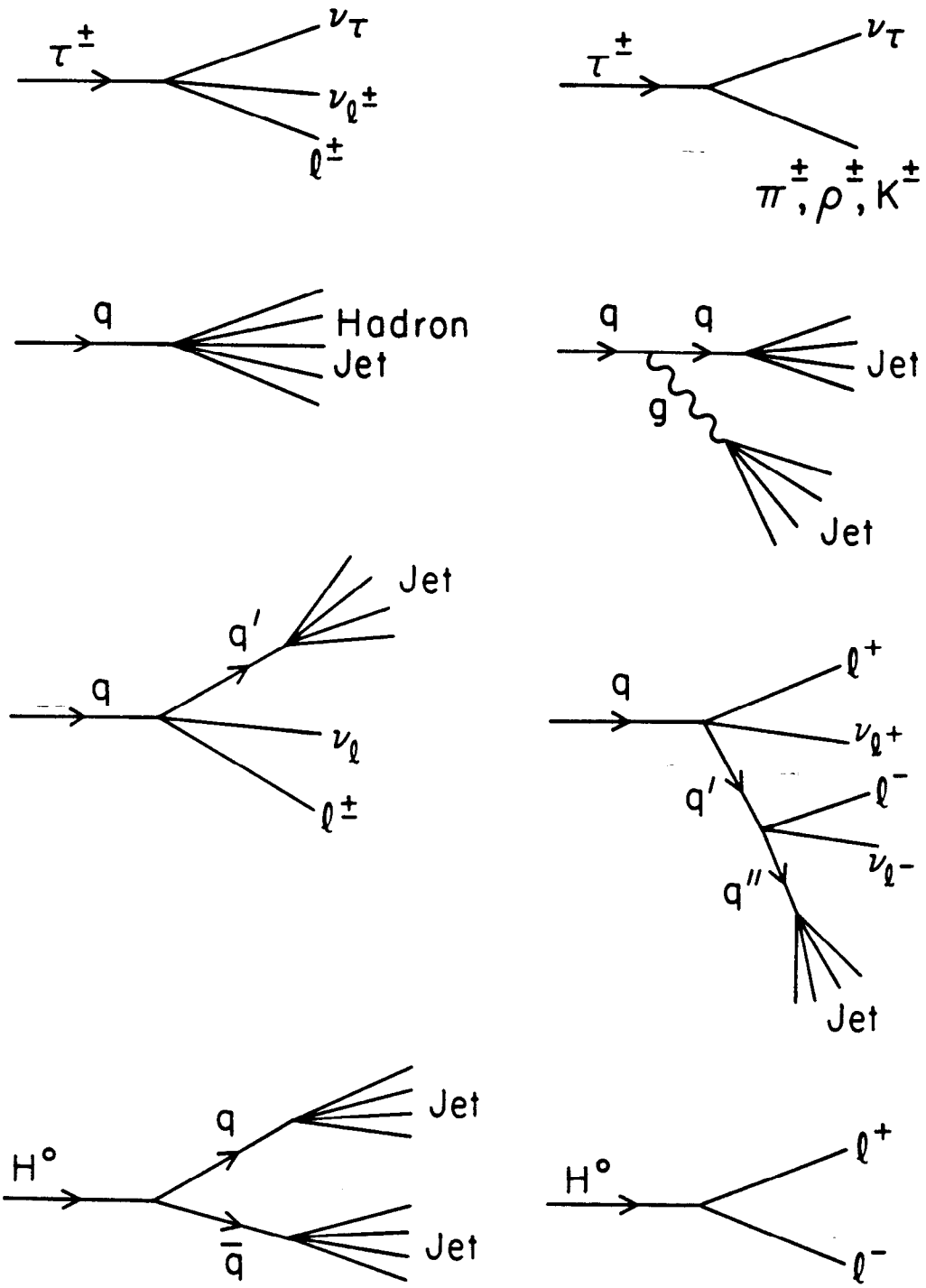
$\tau^{\pm}$
ν_τ
$\nu_\ell^{\pm}$
$\ell^{\pm}$
$\tau^{\pm}$
ν_τ
$\pi^{\pm}, \rho^{\pm}, K^{\pm}$
q
Hadron Jet
q
q
g
Jet
Jet
q
q'
Jet
ν_ℓ
$\ell^{\pm}$
q
ℓ^+
ν_{ℓ^+}
q'
ℓ^-
ν_{ℓ^-}
q''
Jet
H°
q
Jet
$\bar{q}$
Jet
H°
ℓ^+
ℓ^-
4893A2
8-84

Fig. 5

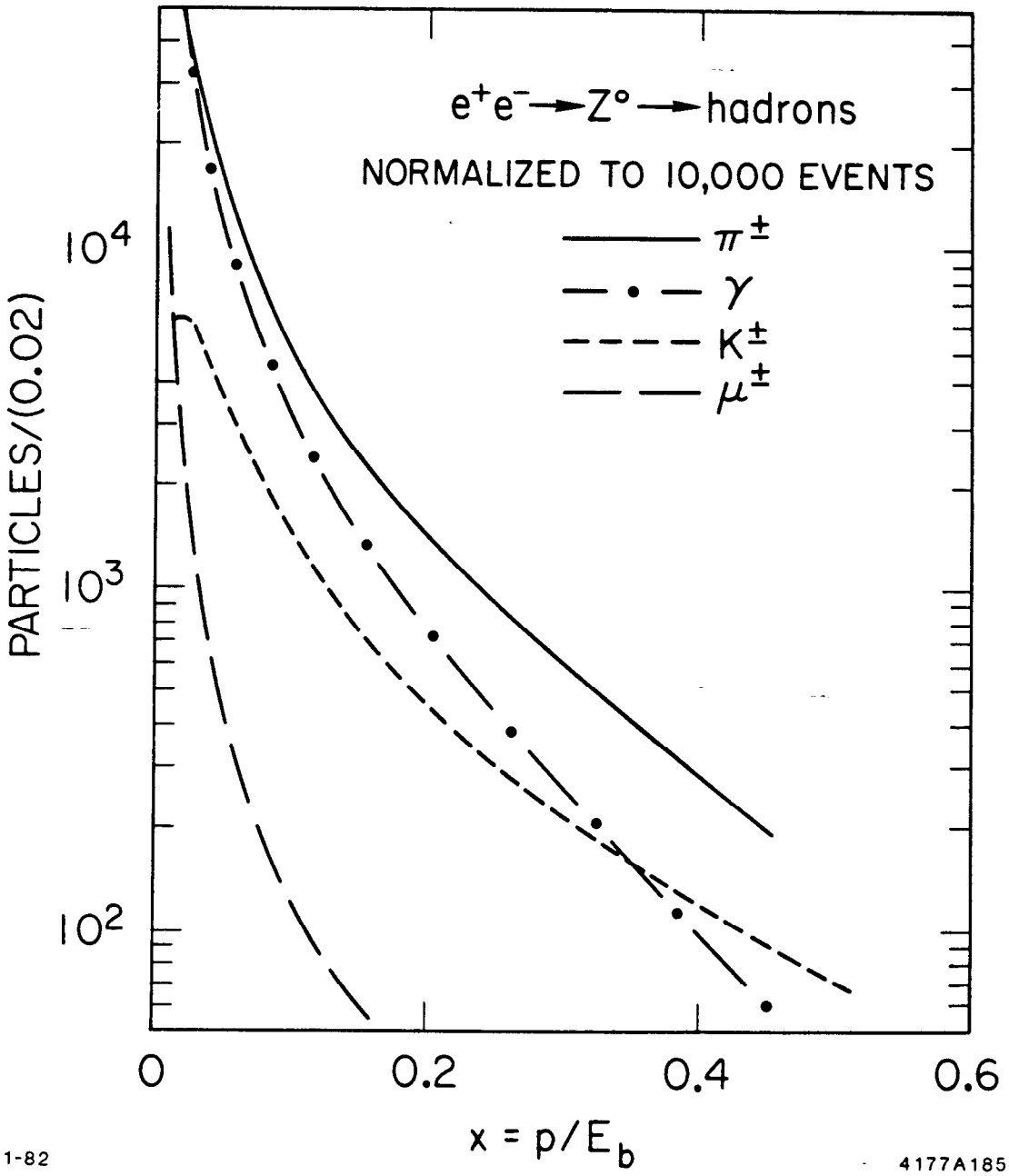
$e^+e^- \rightarrow Z^\circ \rightarrow$ hadrons
NORMALIZED TO 10,000 EVENTS
$\pi^\pm$
γ
$K^\pm$
$\mu^\pm$
PARTICLES/(0.02)
10^4
10^3
10^2
0
0.2
0.4
0.6
$x = p/E_b$
1-82
4177A185

Fig. 6

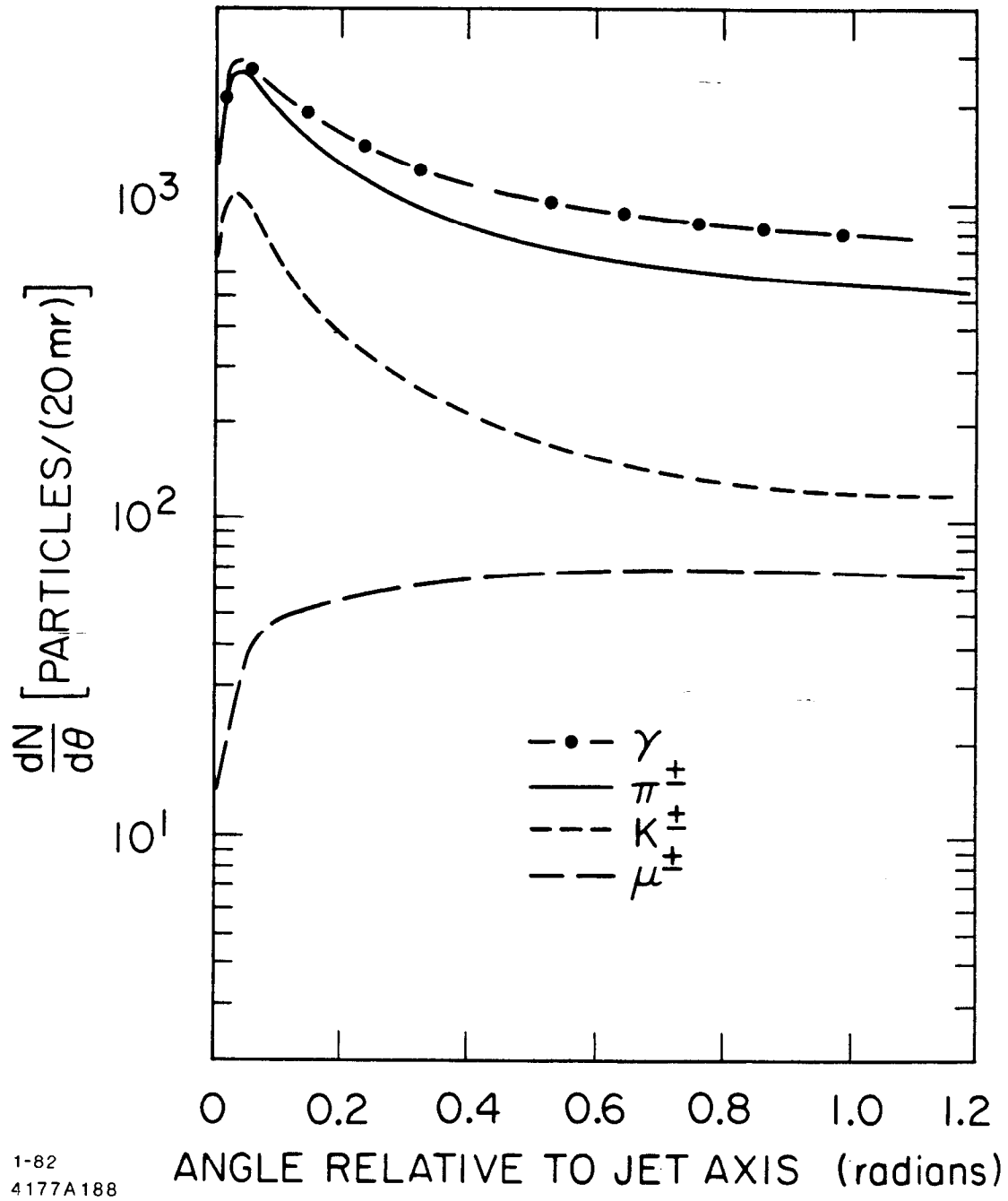
10^3
10^2
10^1
$\frac{dN}{d\theta}$ [PARTICLES/(20 mr)]
γ
$\pi^{\pm}$
$K^{\pm}$
$\mu^{\pm}$
0
0.2
0.4
0.6
0.8
1.0
1.2
ANGLE RELATIVE TO JET AXIS (radians)
1-82
4177A188

Fig. 7

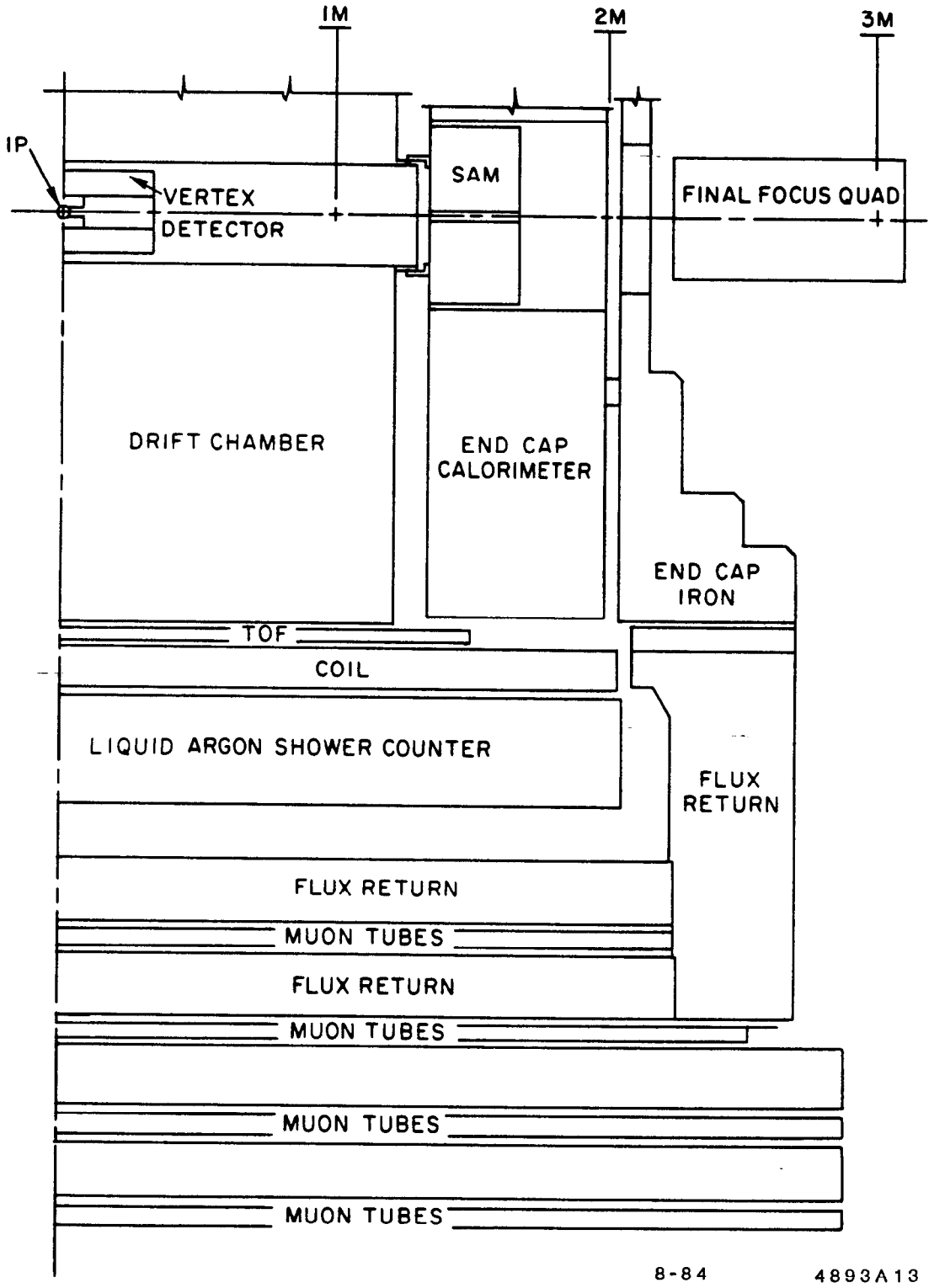
1M
2M
3M
IP
VERTEX
DETECTOR
SAM
FINAL FOCUS QUAD
DRIFT CHAMBER
END CAP
CALORIMETER
END CAP
IRON
TOF
COIL
LIQUID ARGON SHOWER COUNTER
FLUX
RETURN
FLUX RETURN
MUON TUBES
FLUX RETURN
MUON TUBES
MUON TUBES
MUON TUBES
8-84
4893A13

Fig. 8

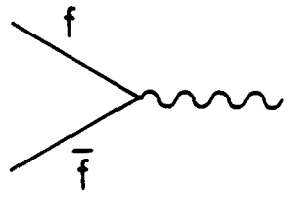

$$-i\,Q_f\,\bar{f}\gamma_\lambda f$$

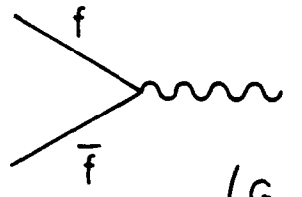

$$-i\sqrt{2}\left(\frac{G_F M_Z^2}{\sqrt{2}}\right)^{1/2}\bar{f}\gamma_\lambda\left[L_f(1-\gamma_5)+R_f(1+\gamma_5)\right]f$$

$$L_f = T_3^f - Q_f \sin^2\theta_W$$

$$R_f = -Q_f \sin^2\theta_W$$

(a)

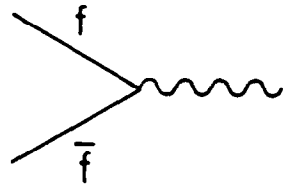

$$-i\,M_f\,(G_F\sqrt{2})^{1/2}$$

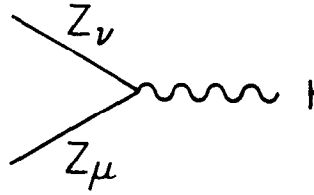

$$-2i\,M_Z^2\,(G_F\sqrt{2})^{1/2}\,g_{\mu\nu}$$

(b)

8-84 4893A3

Fig. 9

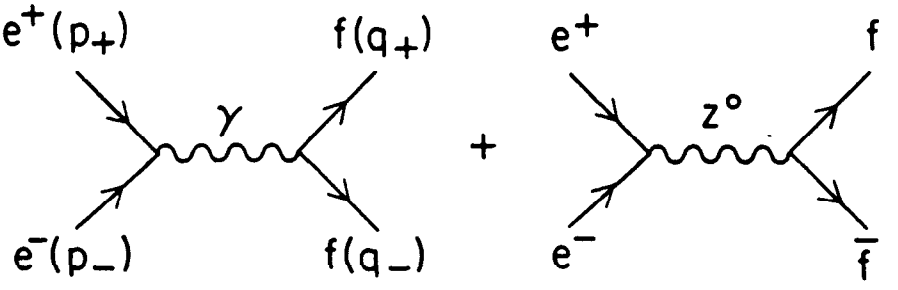

Fig. 10

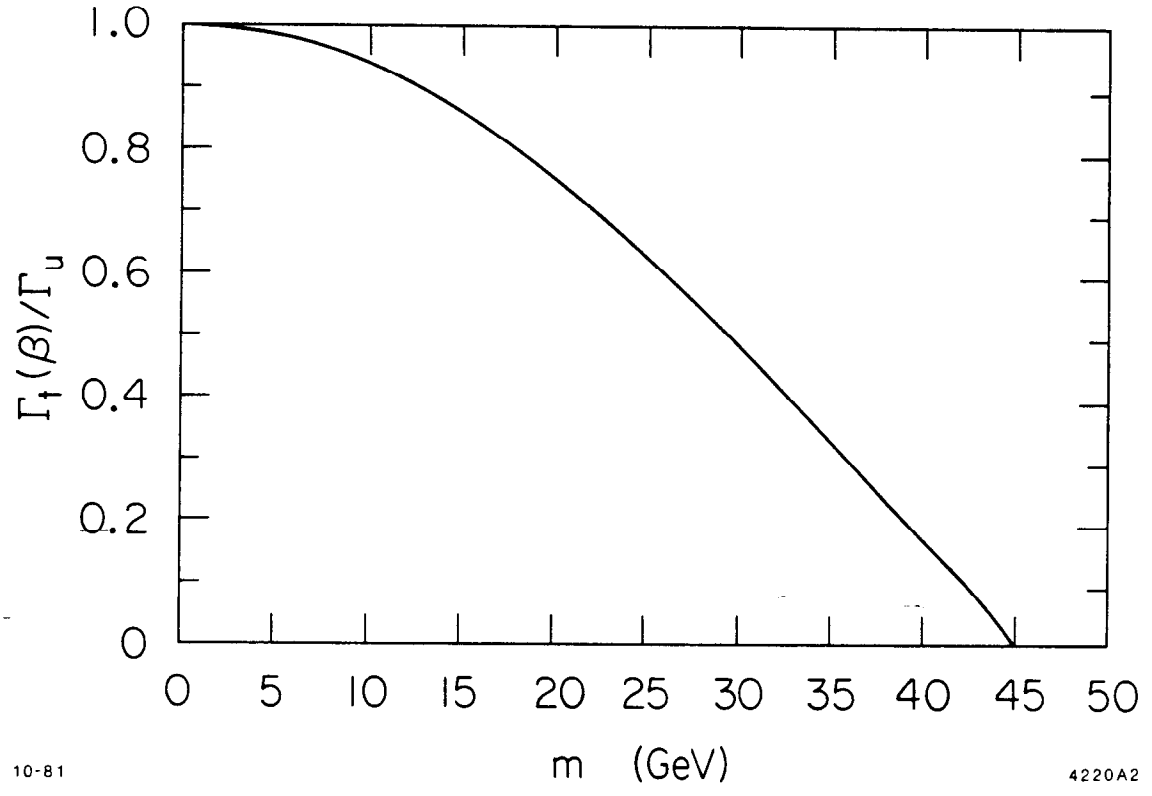
1.0
0.8
0.6
0.4
0.2
0
$\Gamma_f(\beta)/\Gamma_u$
0 5 10 15 20 25 30 35 40 45 50
m (GeV)
10-81
4220A2

Fig. 11

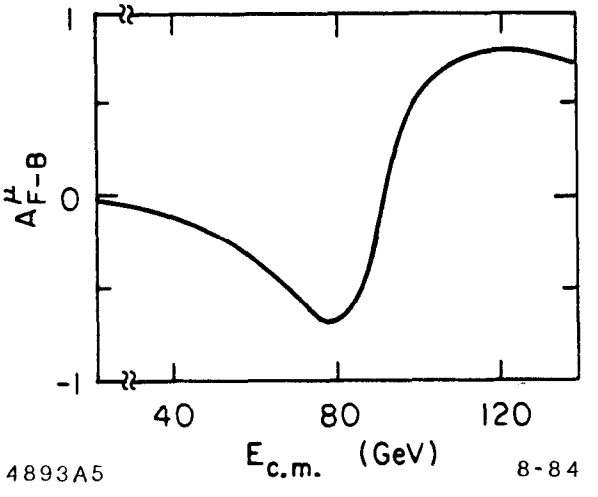

Fig. 12

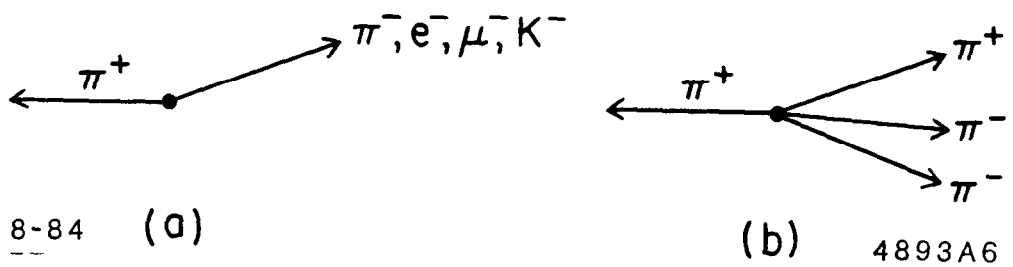

Fig. 13

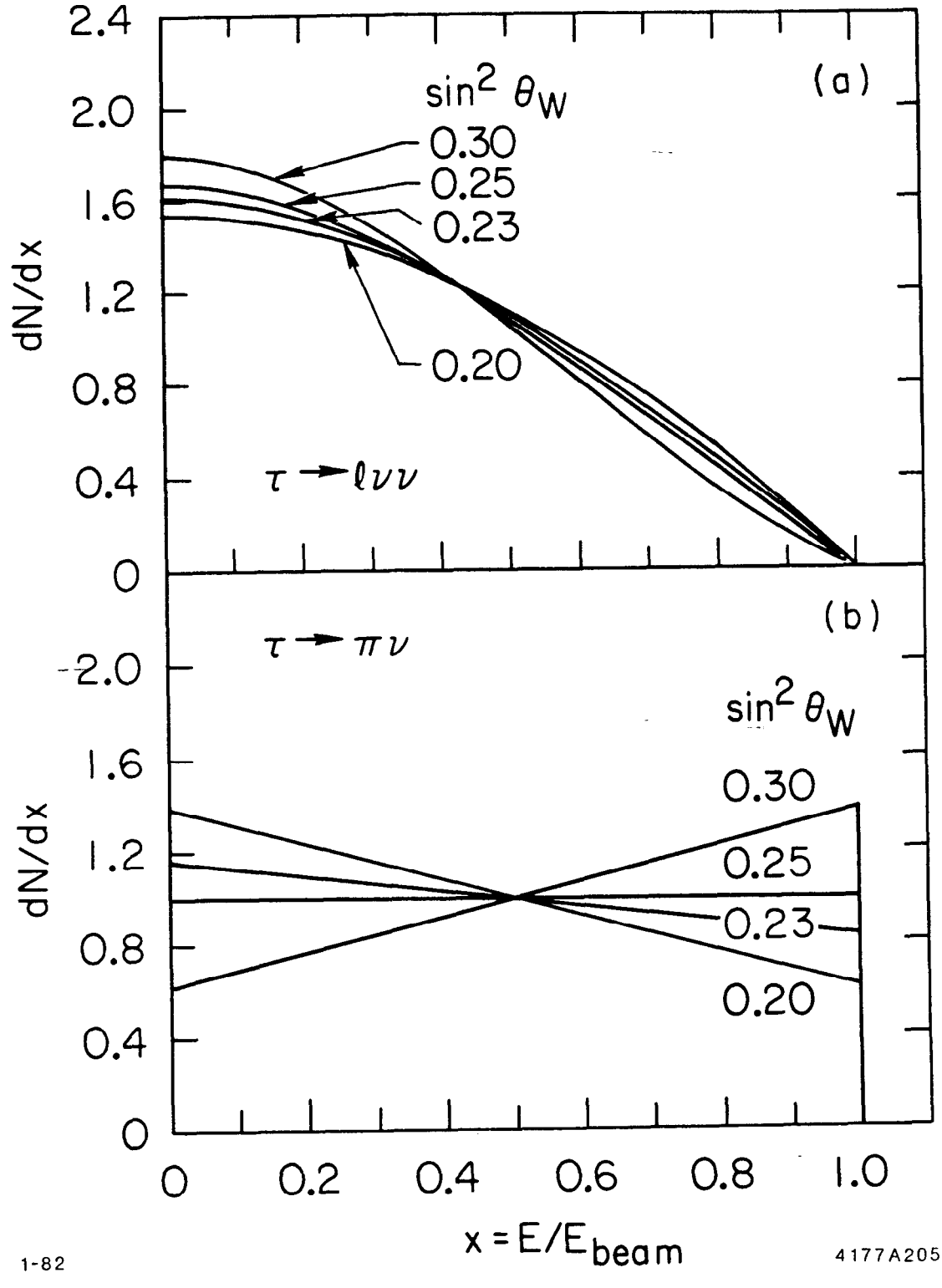
2.4
2.0
1.6
1.2
0.8
0.4
0
dN/dx
sin² θW
(a)
0.30
0.25
0.23
0.20
τ → ℓνν
(b)
τ → πν
-2.0
1.6
1.2
0.8
0.4
0
dN/dx
sin² θW
0.30
0.25
0.23
0.20
0
0.2
0.4
0.6
0.8
1.0
x = E/E beam
1-82
4177A205

Fig. 14

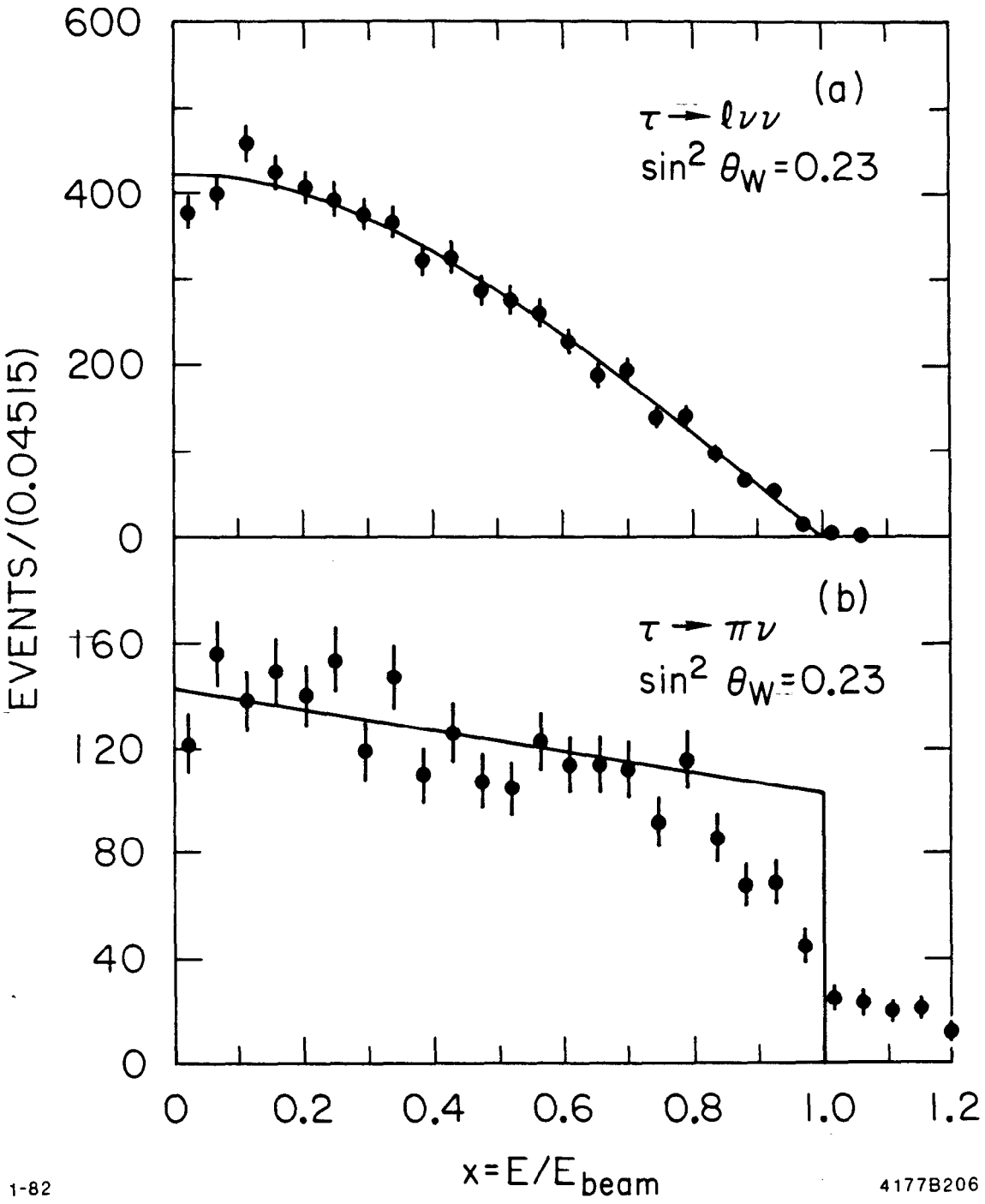
600
400
200
0
(a)
$\tau \rightarrow \ell\nu\nu$
$\sin^2 \theta_W = 0.23$
160
120
80
40
0
(b)
$\tau \rightarrow \pi\nu$
$\sin^2 \theta_W = 0.23$
EVENTS/(0.04515)
0
0.2
0.4
0.6
0.8
1.0
1.2
$x = E/E_{beam}$
1-82
4177B206

Fig. 15

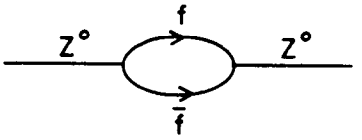

8-84 4893A7

Fig. 16

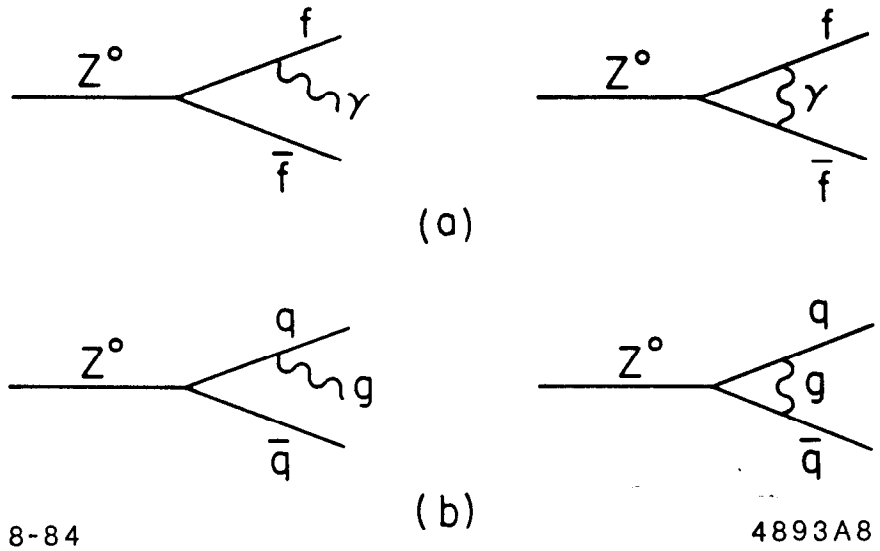

Fig. 17

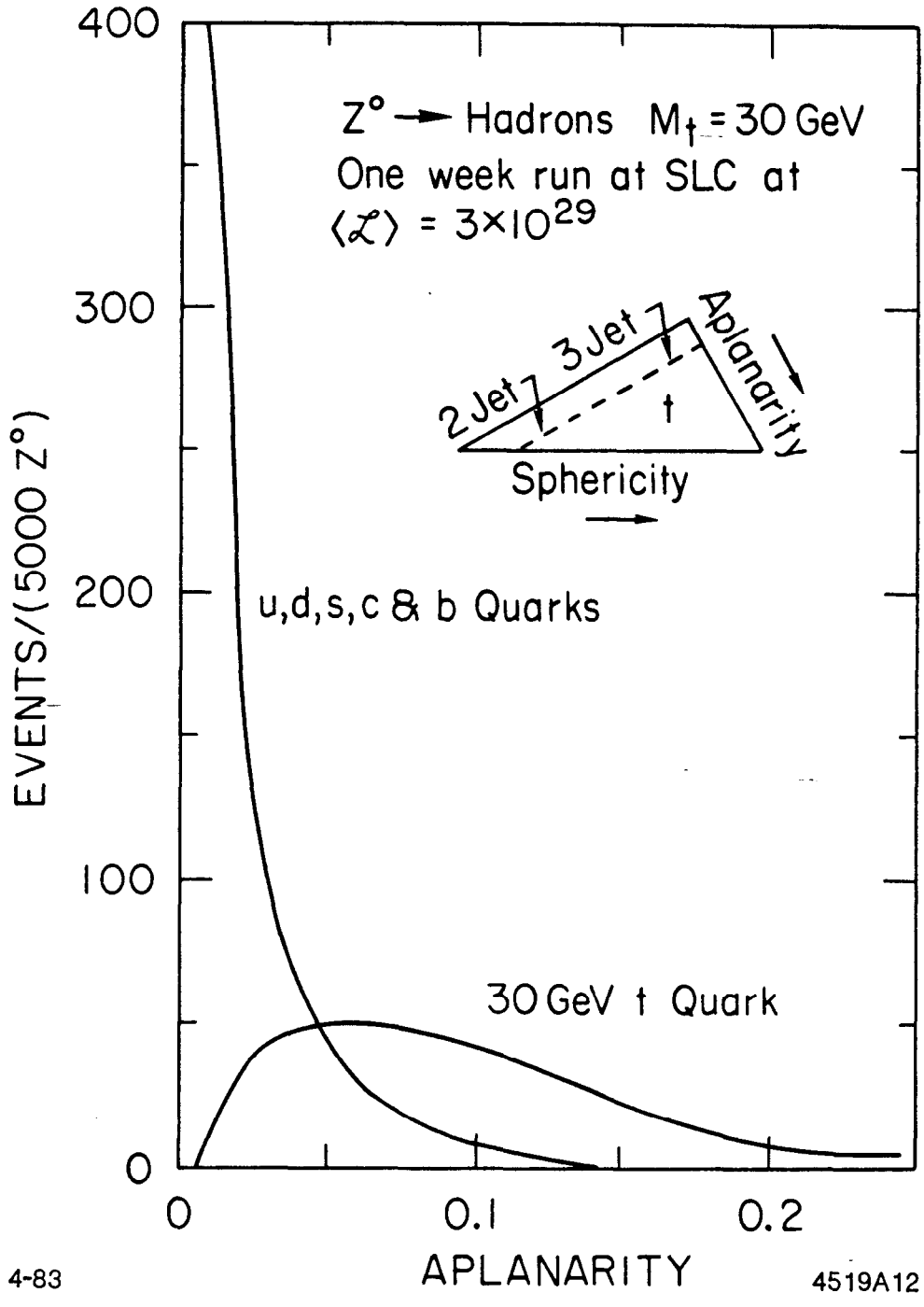
400
300
200
100
0
EVENTS/(5000 Z°)
Z° → Hadrons M_t = 30 GeV
One week run at SLC at
⟨ℒ⟩ = 3×10²⁹
3 Jet
2 Jet
t
Aplanarity
Sphericity
u,d,s,c & b Quarks
30 GeV t Quark
0
0.1
0.2
APLANARITY
4-83
4519A12

Fig. 18

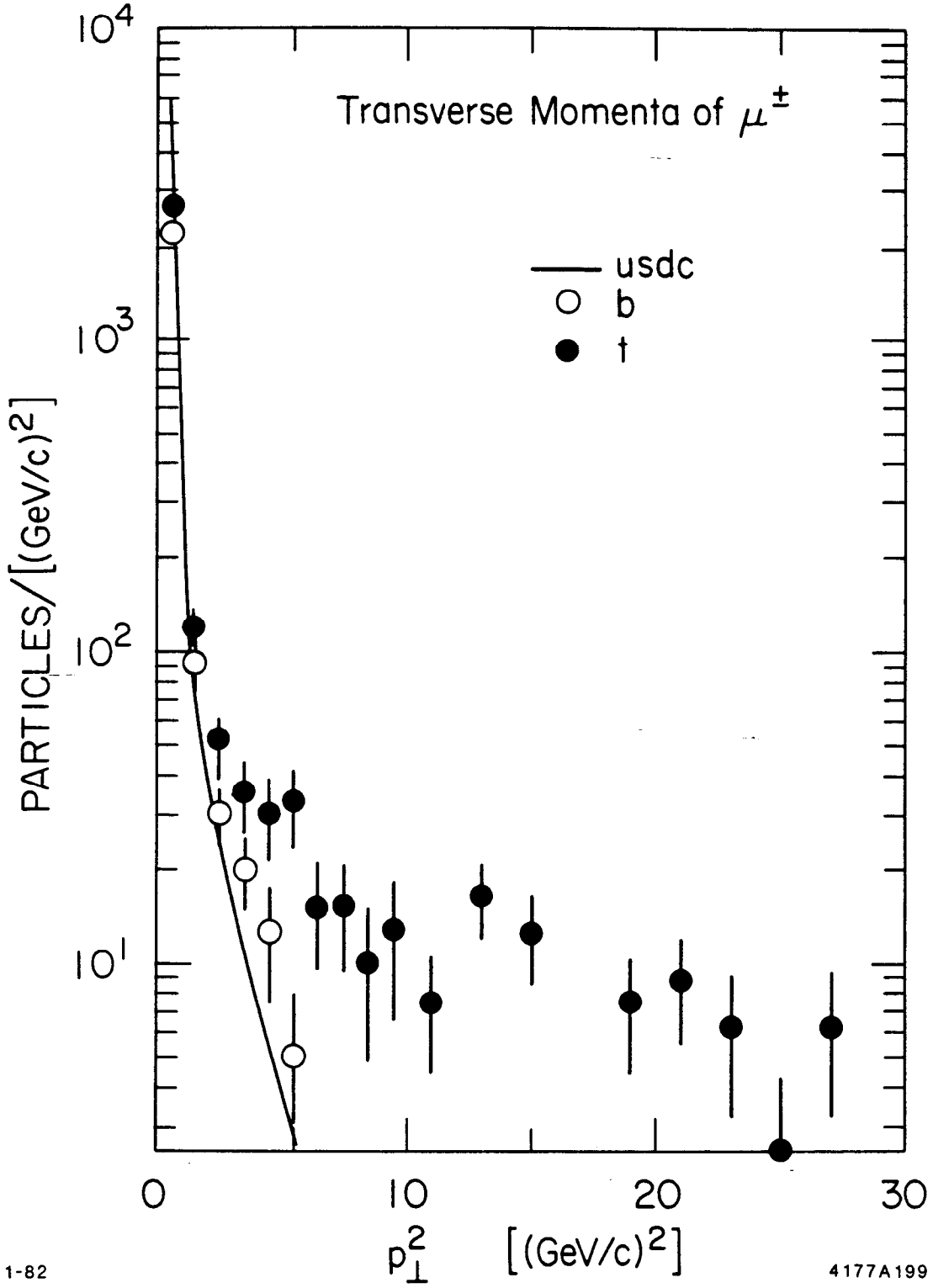
Transverse Momenta of $\mu^{\pm}$
usdc
b
t
PARTICLES/[(GeV/c)^2]
10^4
10^3
10^2
10^1
0
10
20
30
$p_\perp^2$ [(GeV/c)^2]
1-82
4177A199

Fig. 19

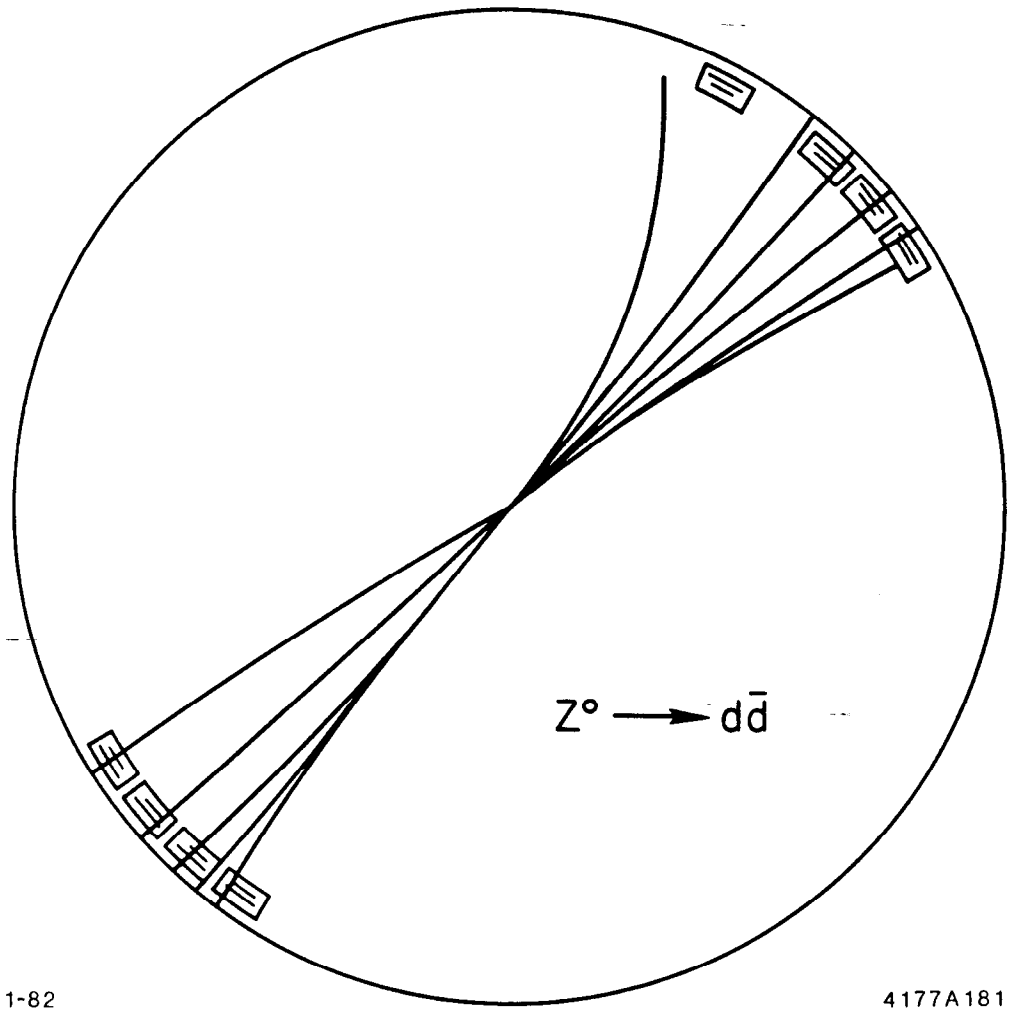

Fig. 20

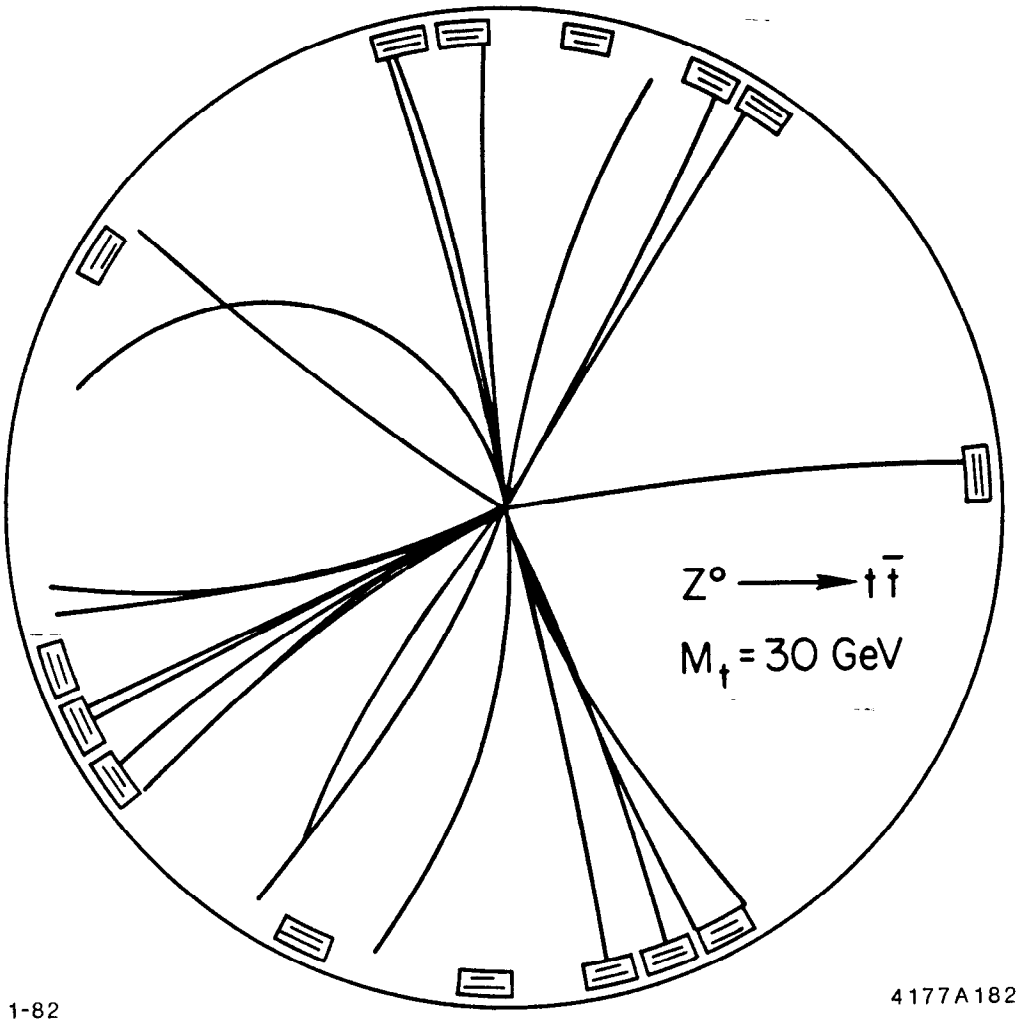

1-82

4177A182

Fig. 21

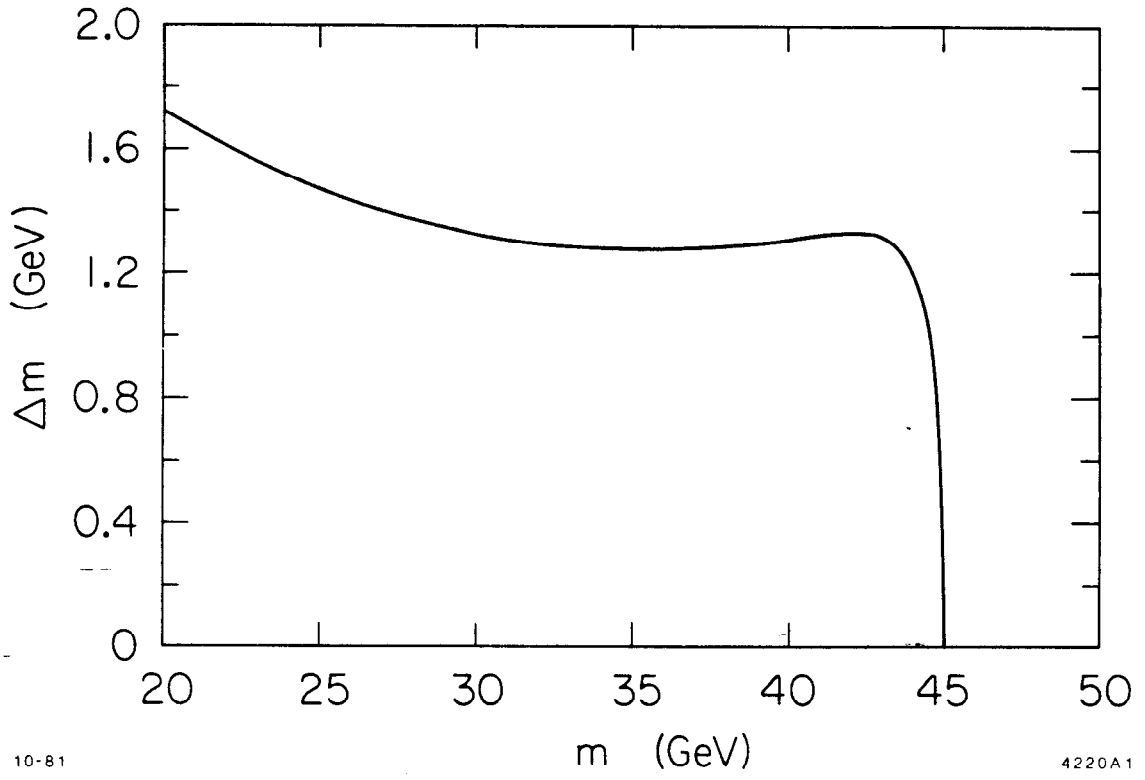

Fig. 22

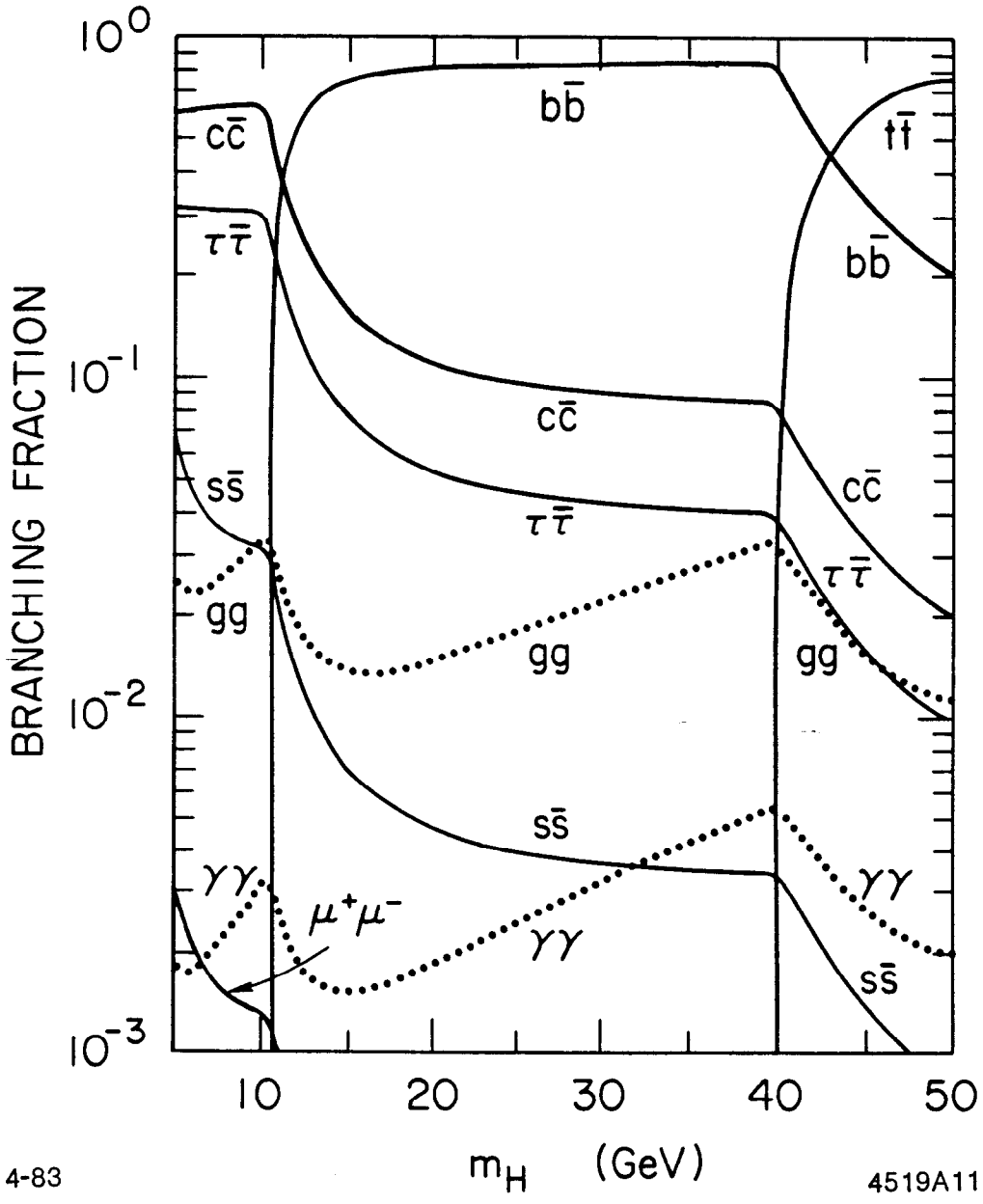
BRANCHING FRACTION
10^0
10^{-1}
10^{-2}
10^{-3}
$b\bar{b}$
$c\bar{c}$
$\tau\bar{\tau}$
$t\bar{t}$
$b\bar{b}$
$c\bar{c}$
$s\bar{s}$
$\tau\bar{\tau}$
$\tau\bar{\tau}$
gg
gg
gg
$s\bar{s}$
$\gamma\gamma$
$\mu^+\mu^-$
$\gamma\gamma$
$\gamma\gamma$
$s\bar{s}$
10
20
30
40
50
m_H (GeV)
4-83
4519A11

Fig. 23

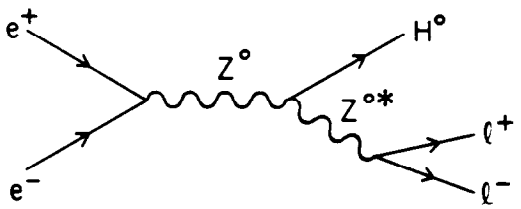

Fig. 24

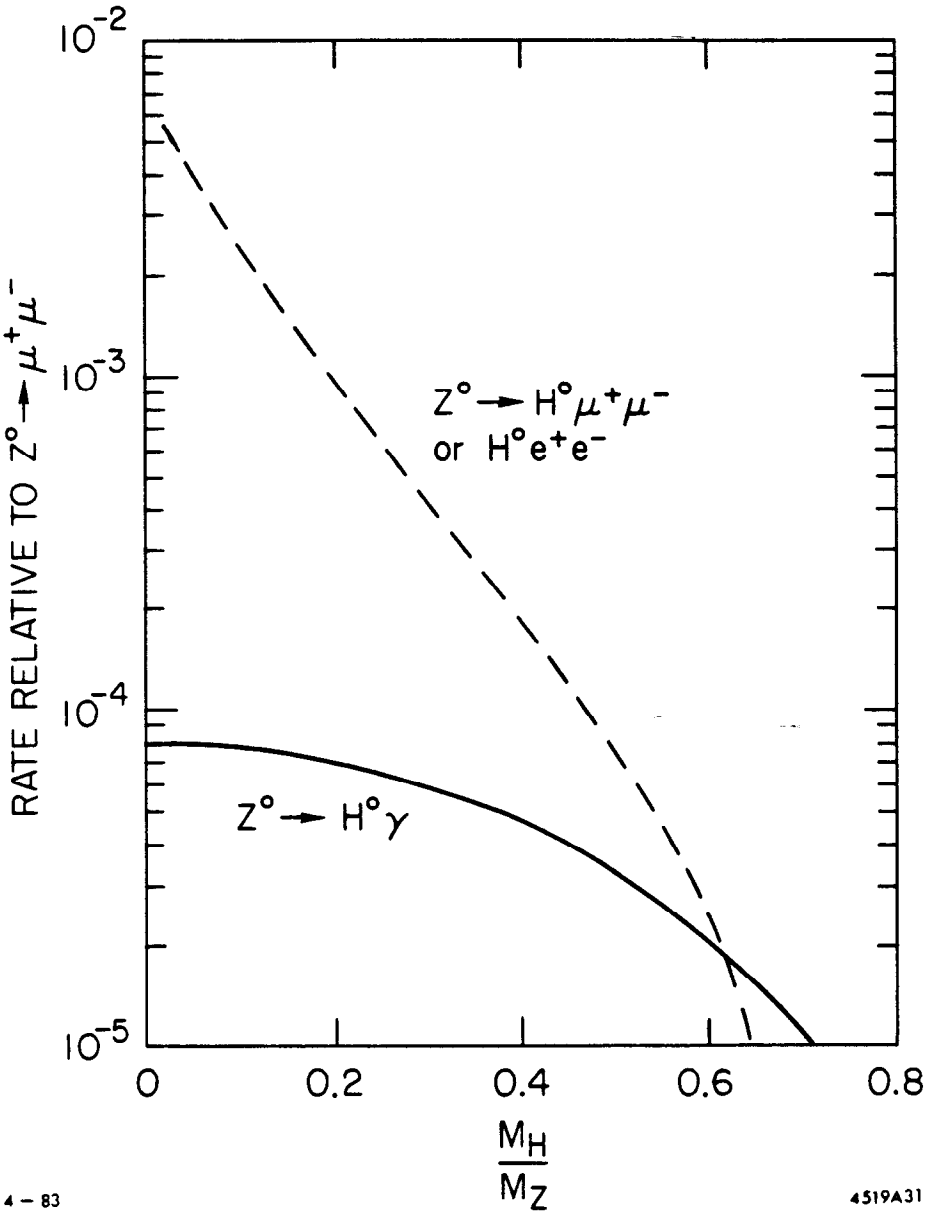
10^{-2}
10^{-3}
10^{-4}
10^{-5}
RATE RELATIVE TO $Z^0 \to \mu^+\mu^-$
$Z^0 \to H^0\mu^+\mu^-$
or $H^0e^+e^-$
$Z^0 \to H^0\gamma$
0
0.2
0.4
0.6
0.8
$\frac{M_H}{M_Z}$
4 – 83
4519A31

Fig. 25

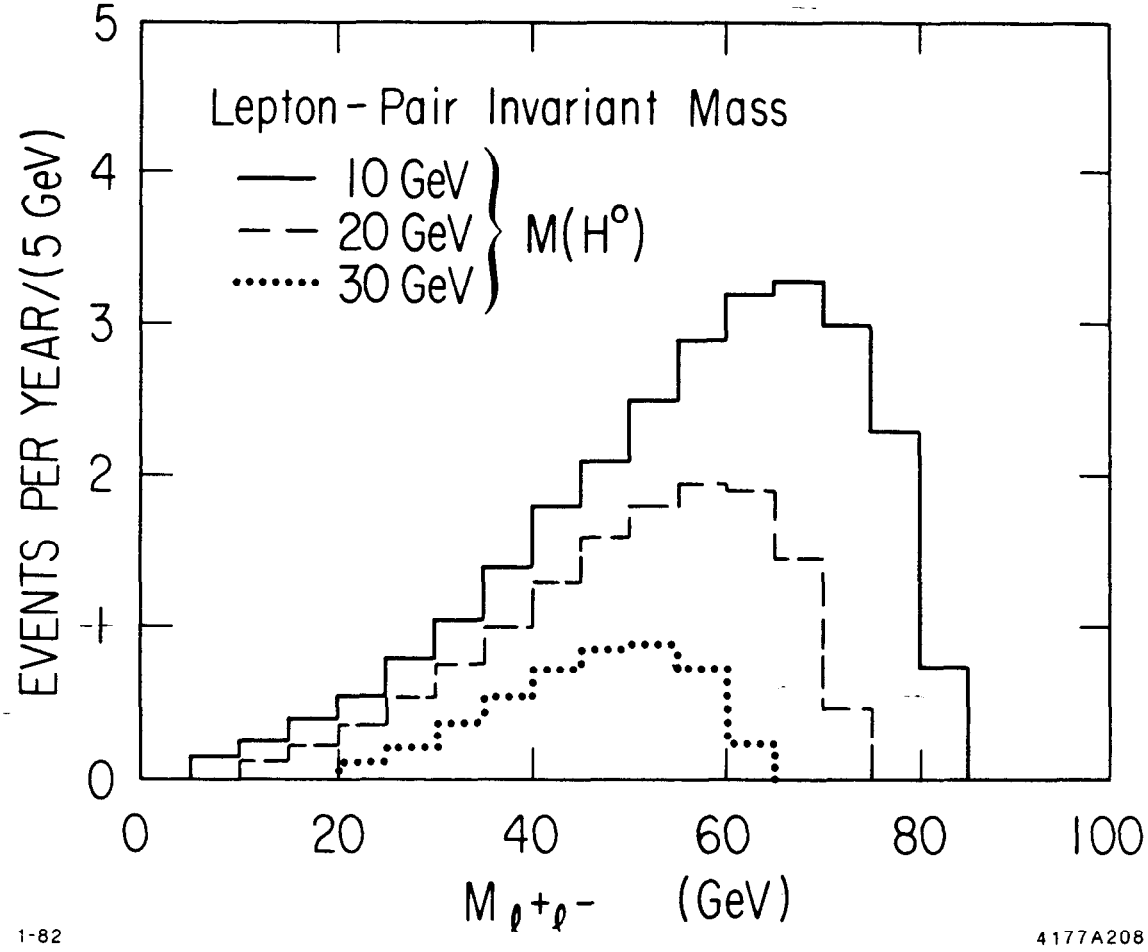
Lepton-Pair Invariant Mass
10 GeV
20 GeV
30 GeV
M(H°)
EVENTS PER YEAR/(5 GeV)
0
1
2
3
4
5
0
20
40
60
80
100
M ℓ+ℓ- (GeV)
1-82
4177A208

Fig. 26

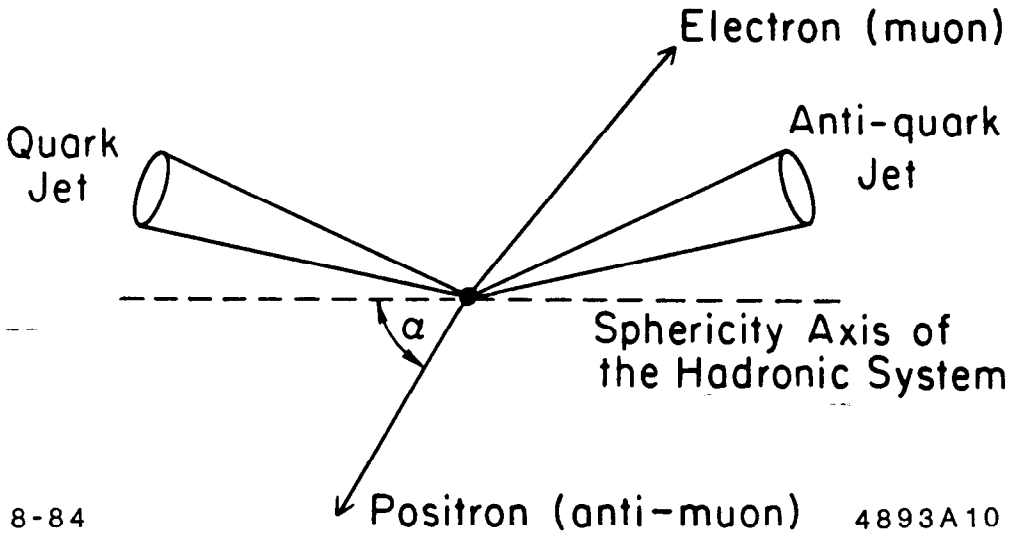
Electron (muon)
Anti-quark
Jet
Quark
Jet
α
Sphericity Axis of
the Hadronic System
Positron (anti-muon)
8-84
4893A10

Fig. 27

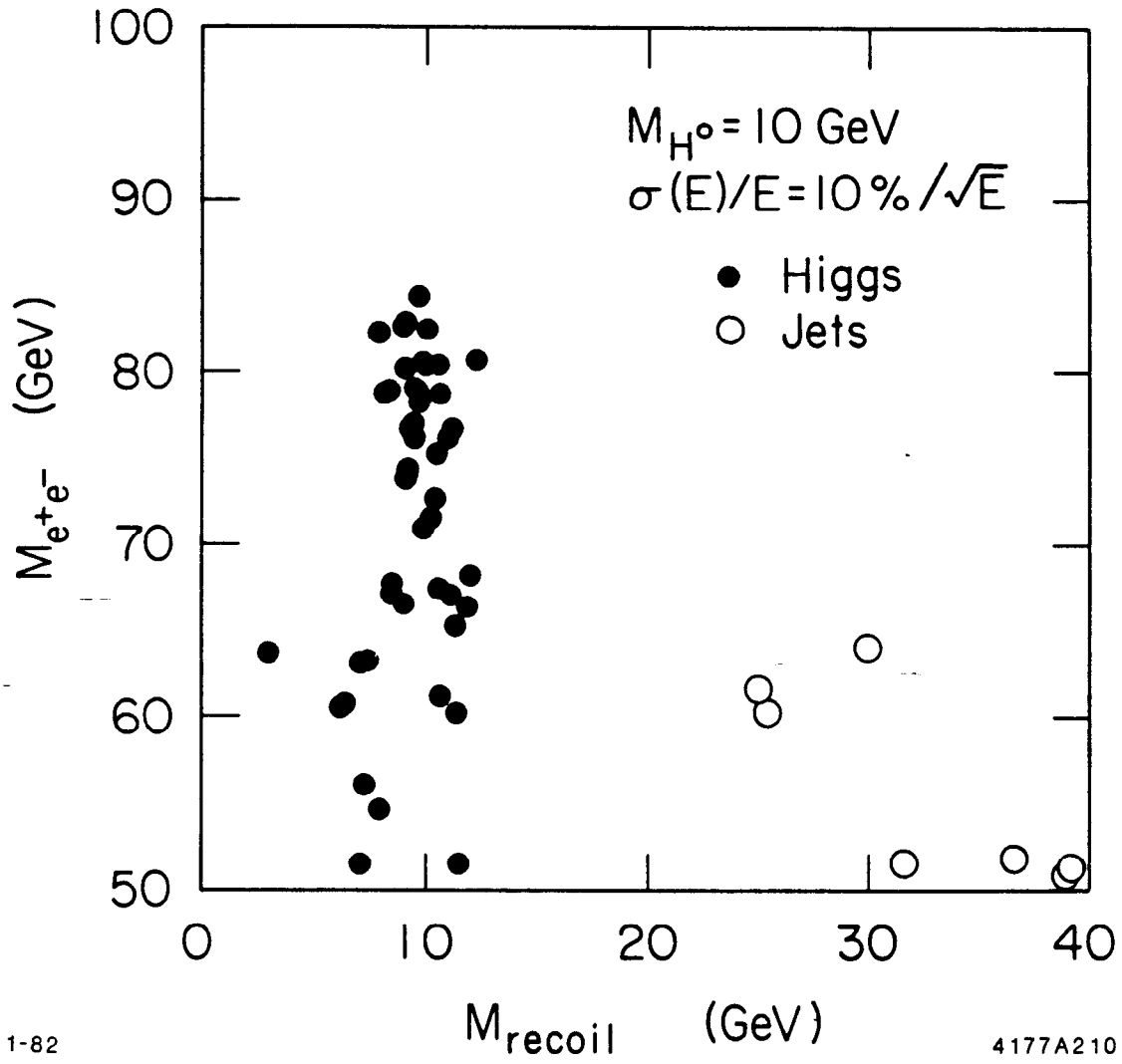
100
90
80
70
60
50
0
10
20
30
40
M_{H^0} = 10 GeV
$\sigma(E)/E = 10\%/\sqrt{E}$
Higgs
Jets
$M_{e^+e^-}$ (GeV)
M_{recoil} (GeV)
1-82
4177A210

Fig. 28

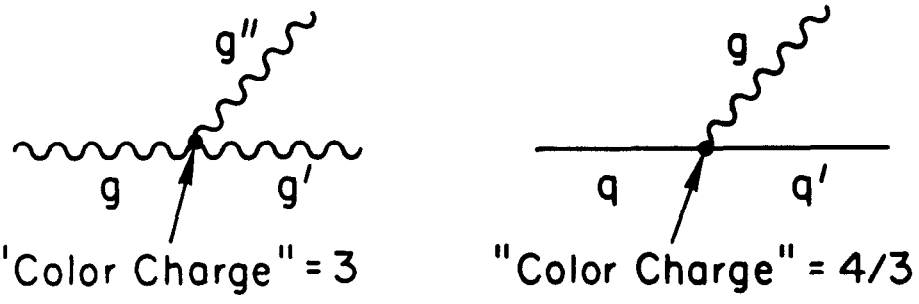

8-84

4893A11

Fig. 29

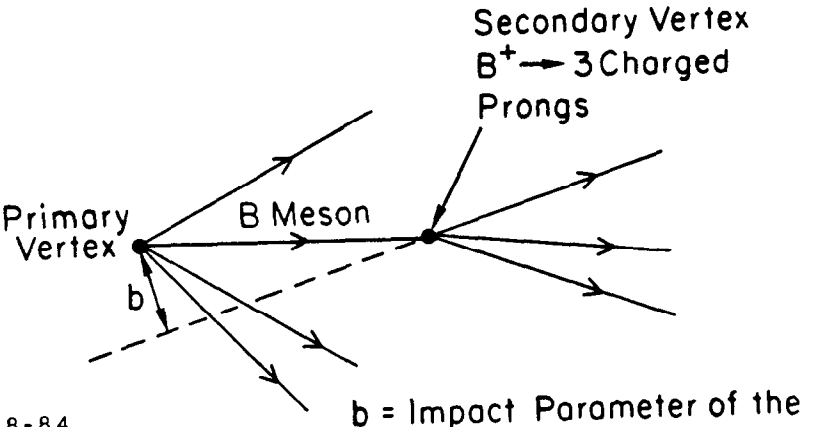
Secondary Vertex
$B^+ \rightarrow$ 3 Charged
Prongs
Primary
Vertex
B Meson
b
b = Impact Parameter of the
B Meson Decay Product
8-84
4893A12

Fig. 30

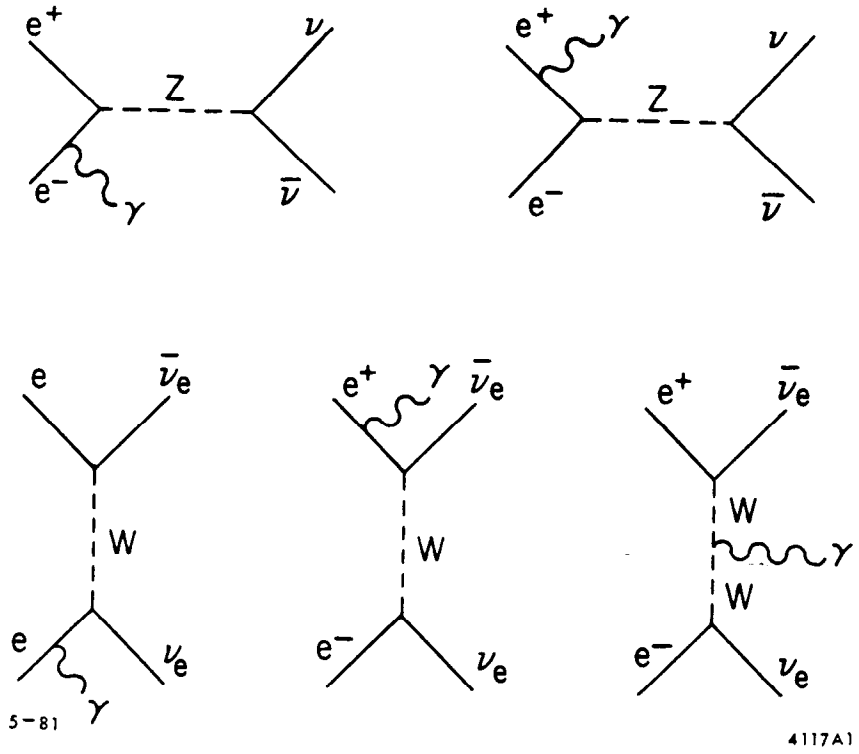

Fig. 31

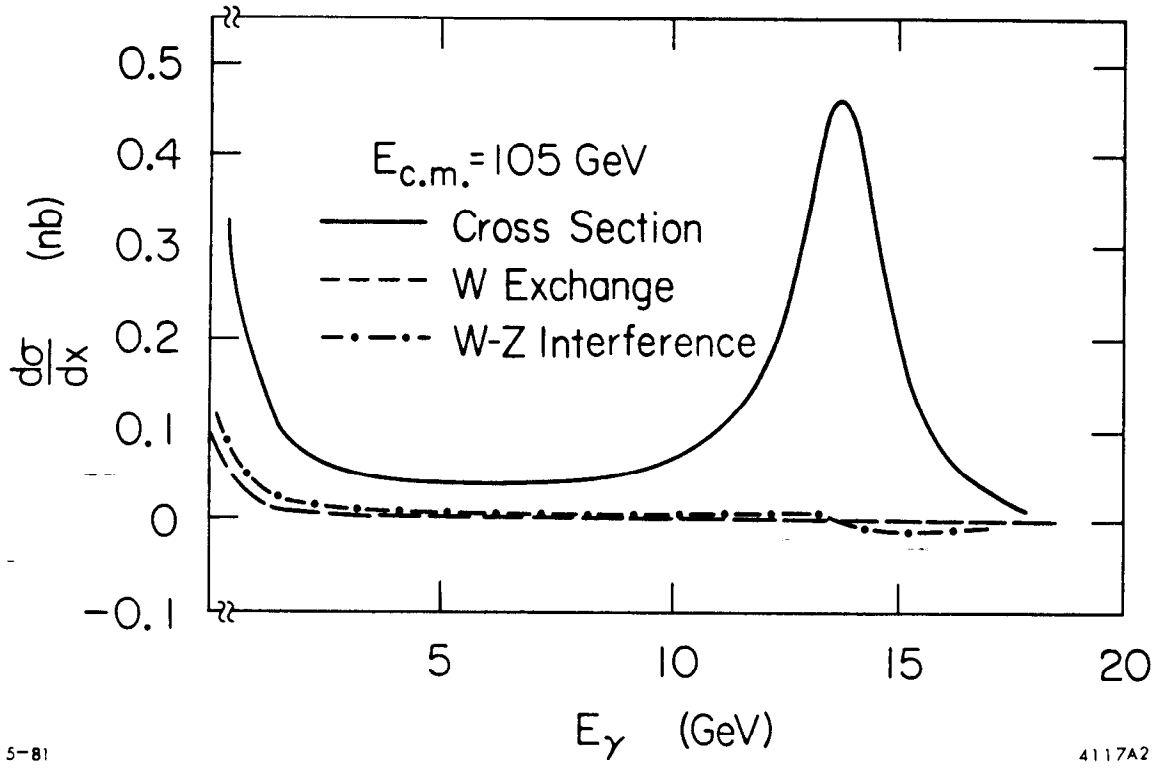
0.5
0.4
0.3
0.2
0.1
0
−0.1
dσ/dx (nb)
E_c.m.=105 GeV
Cross Section
W Exchange
W-Z Interference
5
10
15
20
E_γ (GeV)
5-81
4117A2

Fig. 32

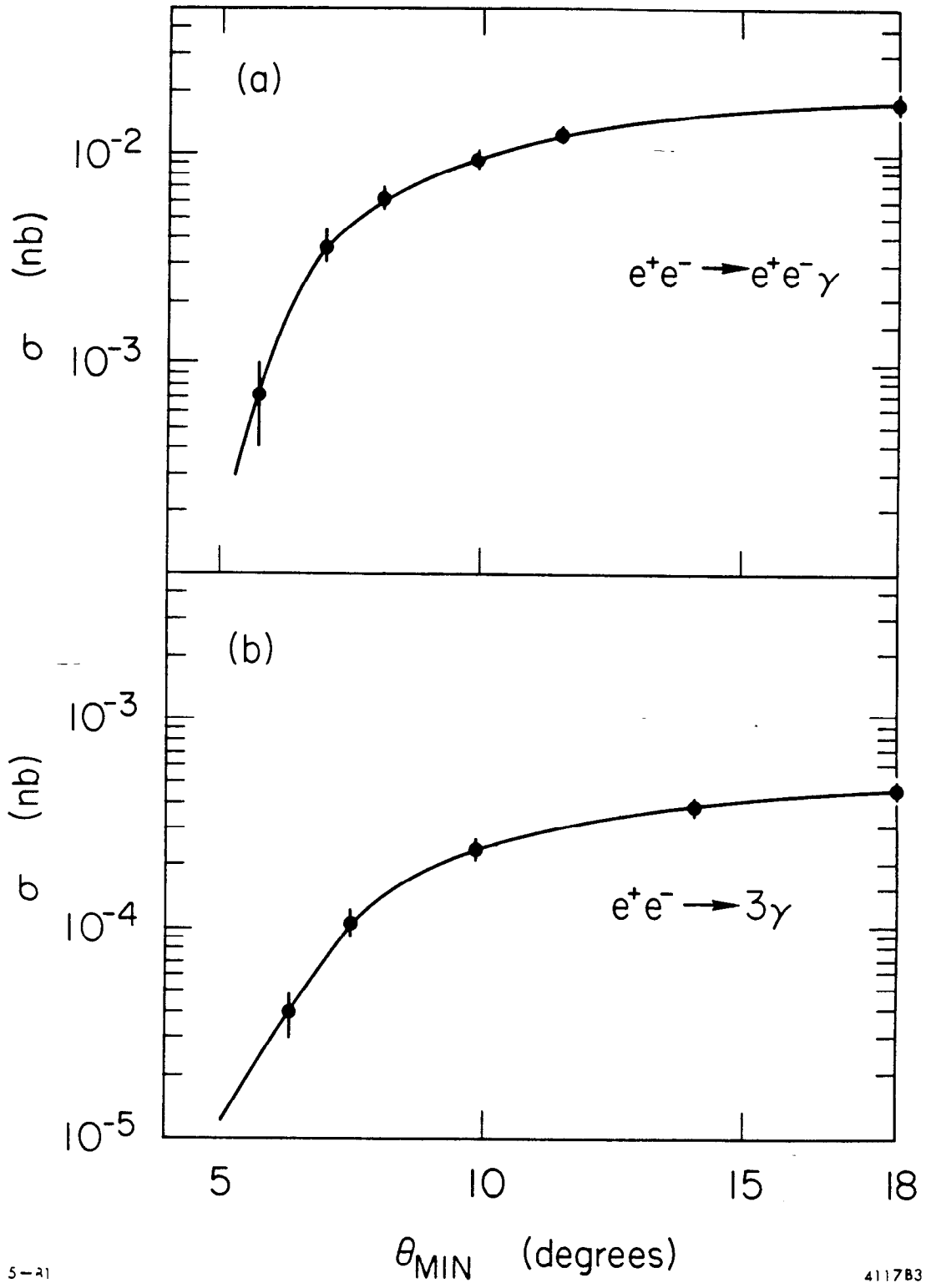
(a)
10^{-2}
10^{-3}
σ (nb)
$e^+e^- \rightarrow e^+e^-\gamma$
(b)
10^{-3}
10^{-4}
10^{-5}
σ (nb)
$e^+e^- \rightarrow 3\gamma$
5
10
15
18
θ_{MIN} (degrees)
5-81
411783

Fig. 33

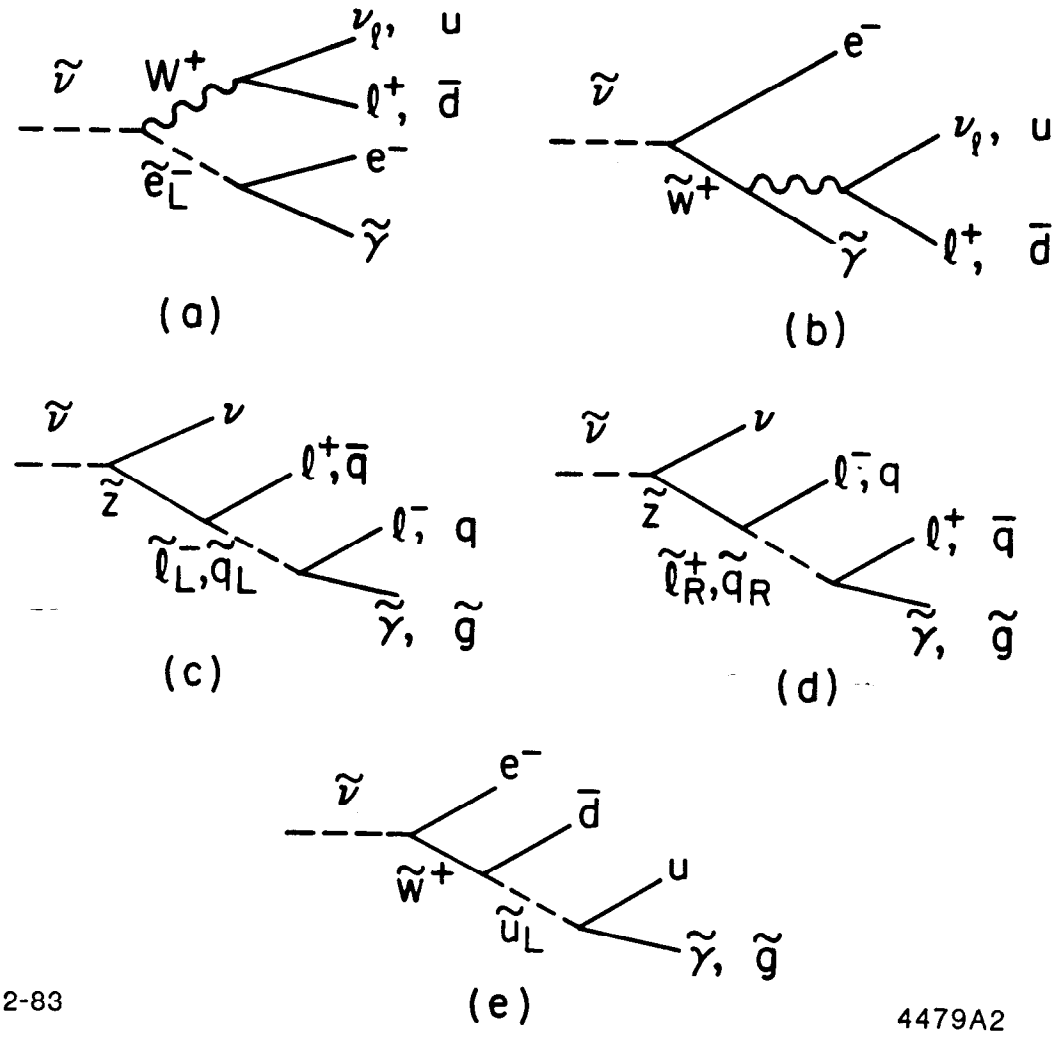
$\tilde{\nu}$
W^+
ν_ℓ, u
ℓ^+, $\bar{d}$
$\tilde{e}_L^-$
e^-
$\tilde{\gamma}$
(a)
$\tilde{\nu}$
e^-
$\tilde{W}^+$
ν_ℓ, u
$\tilde{\gamma}$
ℓ^+, $\bar{d}$
(b)
$\tilde{\nu}$
ν
$\tilde{z}$
ℓ^+,$\bar{q}$
$\tilde{\ell}_L^-$,$\tilde{q}_L$
ℓ^-, q
$\tilde{\gamma}$, $\tilde{g}$
(c)
$\tilde{\nu}$
ν
$\tilde{z}$
ℓ^-,q
$\tilde{\ell}_R^+$,$\tilde{q}_R$
ℓ^+, $\bar{q}$
$\tilde{\gamma}$, $\tilde{g}$
(d)
$\tilde{\nu}$
e^-
$\bar{d}$
$\tilde{W}^+$
u
$\tilde{u}_L$
$\tilde{\gamma}$, $\tilde{g}$
(e)
2-83
4479A2

Fig. 34